Engineering topological phases of any winding and Chern numbers in extended Su-Schrieffer-Heeger models

Rakesh Kumar Malakar[1,*] and Asim Kumar Ghosh[1,†]

[1]*Department of Physics, Jadavpur University, 188 Raja Subodh Chandra Mallik Road, Kolkata 700032, India*

Simple route of engineering topological phases for any desired value of winding and Chern numbers is found in the Su-Schrieffer-Heeger (SSH) model by adding a further neighbor hopping term of varying distances. It is known that the standard SSH model yields a single topological phase with winding number, $\nu = 1$. In this study it is shown that how one can generate topological phases with any values of winding numbers, for examples, $\nu = \pm1, \pm2, \pm3, \cdots$, in the presence of a single further neighbor term which preserves inversion, particle-hole and chiral symmetries. Quench dynamics of the topological and trivial phases are studied in the presence of a specific nonlinear term. Another version of SSH model with additional modulating nearest neighbor and next-nearest-neighbor hopping parameters was introduced before which exhibit a single topological phase characterized by Chern number, $\mathcal{C} = \pm1$. Standard form of inversion, particle-hole and chiral symmetries are broken in this model. Here this model has been studied in the presence of several types of parametrization among which, for a special case the system is found to yield a series of phases with Chern numbers, $\mathcal{C} = \pm1, \pm2, \pm3, \cdots$. In another parametrization, multiple crossings within the edge states energy lines are found in both trivial and topological phases. Topological phase diagrams are drawn for every case. Emergence of spurious topological phases is also reported.

Corresponding author: Asim Kumar Ghosh

PACS numbers:

I. INTRODUCTION

Su-Schrieffer-Heeger (SSH) model is the most popular representative of one-dimensional (1D) topological insulator which paved the way for studying the topological phases in the simplest manner[1,2]. Both trivial and topological insulating phases have been realized by tuning the ratio of inter and intracell hopping amplitudes in this staggered model composed by two-site unit cells. Nontrivial phase is observed when this ratio exceeds unity and it is characterized by a nonzero topological invariant known as winding number (ν) which is connected to the integral of Berry curvature over the Brillouin zone (BZ) and known as Pancharatnam-Berry (PB) phase or Zak phase. This nontrivial phase is at the same time associated with the emergence of symmetry protected zero energy states which are found localized on both the edges of the open chain. Transition between those two phases with nonzero band gap is accompanied by vanishing band gap found at the phase transition point.

SSH model is connected with the 1D Kitaev model by unitary transformation, which opens up a new field of investigation known as topological superconductivity[3]. Importance of topological matter lies in the fact that additional topological robustness in the nontrivial phase protects these systems from any kind of imperfections present in the materials. This robustness enhances quantum correlations[4] and causes higher efficiency in electronic transport. As a result, topological materials are expected to be more suitable in the development of quantum processing devices[5].

SSH model was introduced before in a totally different context, as it was employed to understand the role of solitonic excitations in conducting polymers, like polyacetylene, etc. The PB phase has been measured recently by mimicking the 1D periodic potential of polyacetylene using system of ultracold atoms in optical lattices[6]. Signature of topologically protected pair of bound states is also detected by photonic quantum walk[7]. In addition, properties of tight-binding SSH model have been experimentally validated in photonic lattice composed of helical waveguides[8] and in phononic crystal composed of cylindrical waveguides[9].

Existence of topological phase has been demonstrated in various SSH-like dimerized models in numerous investigations. For example, in a non-Hermitian SSH model, where intracell hopping term is turned imaginary keeping the intercell hopping real, the same type of topological behaviour is obtained[10]. The same topological phase appears again in another dimerized model constituted by bigger unit cell comprising of four lattice points[11,12]. In another study, existence of anomalous Floquet topological π mode is successfully demonstrated in periodically driven SSH model[13]. Topological properties of a hybrid system comprised of SSH and Kitaev models are studied in order to find the role of particle-hole symmetry embedded in the individual models[14]. Another type of SSH-like staggered model, where particle number is not conserved is employed before in order to study its quantum phase transition along with to explain the nontrivial quench during the transition[15,16]. However, most of these models incorporate no further neighbor hopping term. At the same time it is also true that no topological phase with $\nu > 1$ appears without further neighbor terms.

The topological phase in two-band SSH model is defined uniquely by $\nu = 1$ for each band. Besides, search of new topological phases, preferably with higher values of ν continues afterwards by adding further neighbor hopping terms. Collectively they are called extended SSH (eSSH) models. Emergence of a new phase with $\nu = -1$ has been demonstrated before by adding a single further neighbor hopping term[17]. In another investigation, additional phase with $\nu = 2$ has been obtained simply by adding a pair of staggered further neighbour terms[11]. By invoking multiple further neighbor hopping terms new phases with $\nu = 2, 3, 4$ have been generated later[18,19]. PB phase of eSSH model is determined with the Wannier functions by taking into account the different postions for two sites within the unit cell[20]. Emergence of multiple topological phases in Kitaev chain with long range couplings is reported before[21]. In this work it is shown that the eSSH model is capable to host indefinite number of topological phases with a series of different winding numbers as one wishes. And remarkably, in this series of eSSH models only a single extra further neighbor hopping term is sufficient for their realization.

Interestingly, demonstration of topological phases in two-dimensional (2D) system has been started, long before, with the discovery of integer quantum Hall effect[22,23]. Subsequently, this phenomenon is observed in other systems as well, when Haldane found its realization on a tight-binding model with complex further neighbor hopping terms formulated on honeycomb lattice[24]. This finding gives birth to new area of research known as quantum anomalous Hall (QAH) effect where the magnetic field is replaced by phase dependent hoppings. This state of matter was experimentally realized in periodically modulated optical honeycomb lattice[25]. For the 2D systems, Chern number $\mathcal{C}$, is treated as the topological invariant. In the two-band Haldane model, topological phase is defined by $\mathcal{C} = \pm 1$, values of opposite signs for the two different energy bands. Realization of topological phase for higher values of $\mathcal{C}$s continues thereafter by either invoking further neighbour hopping terms[26–28] or imposing periodic drive[29,30], etc. Experimental realization of QAH phases tunable up to $\mathcal{C} = \pm 5$ has been reported recently[31].

In another development, finding of QAH effect breaks its dimensional barrier, as the realization of this phase is possible in 1D eSSH model, where nearest neighbor (NN) and next-nearest-neighbor (NNN) hopping amplitudes are modulated by two independent cyclic variables[32]. Remarkably, in this case, one of the cyclic variable can be treated like an additional synthetic dimension. So as a whole, this 1D model behaves like an effective 2D model in the reciprocal space and at the same time, hosts nontrivial topological phases.

Again, in this investigation, the eSSH models are studied in 2D reciprocal space by introducing different kind of parametrization in terms of those two cyclic parameters. And again, it is shown that these models are capable to host indefinite number of topological phases with a series of different Chern numbers. Properties of these new phases with higher values of $\mathcal{C}$s have been characterized in details. Article has been organized in the following manner.

Structure of these eSSH models are described in the section II. Topological phases of eSSH models are characterized in Sec. III. Four different eSSH models are introduced here, whose topological properties are studied in details in terms of winding numbers, edge states, and quench dynamics. Models for phases of higher values of ν will be generalized at the end of this section. Topological phases in terms of Chern numbers are studied in Sec. IV. Several types of parametrization are introduced and their topological properties are characterized. Spurious topological phases are identified. Topological phase diagrams have been drawn in very case and the symmetries of the Hamiltonian are explained. A discussion based on these results is available in Sec V.

II. SSH MODELS WITH FURTHER NEIGHBOR TERMS

The standard SSH model[1] is defined on a 1D bipartite lattice where one primitive cell contains two different sites, A and B. The corresponding Hamiltonian is described as

$$H_{vw} = \sum_{j=1}^{N} \left(v\, c^{\dagger}_{\mathrm{A},j} c_{\mathrm{B},j} + w\, c^{\dagger}_{\mathrm{A},j+1} c_{\mathrm{B},j} \right) + \mathrm{h.c.}, \quad (1)$$

where $c_{\mathrm{A},j}$ and $c_{\mathrm{B},j}$ stand for the annihilation operators of electron on sublattices A and B, respectively, in the jth primitive cell. N is the total number of primitive cells where v and w are the intracell and intercell hopping amplitudes, respectively. These terms permit hopping only between the adjacent sites. Energy spectrum of H_{vw} is gapless when $w = v$, while there is a band gap when $w \neq v$. Between the two gapful regions around the gapless point, one is topologically trivial ($\nu = 0$) when $w < v$, and remarkably as long as $w > v$, this simple model hosts a single nontrivial topological phase with $\nu = 1$.

In 2019, Li and Miroshnichenko[17] showed that a new topological phase with $\nu = -1$ appears on introducing additional terms which allow hopping between sites of A sublattice and nonadjacent sites of B sublattice but only among the NN primitive cells as shown in Fig. 1. A single pair of topological edge states is found to appear associated with this new phase.

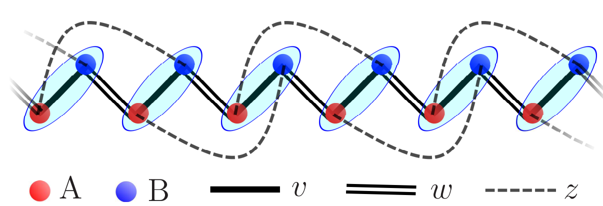

FIG. 1: Extended SSH model describing the hopping for the total Hamiltonian, H, in Eq. 2.

The chiral symmetry of the resultant system is preserved by this specific choice of sites between which the hopping is allowed. If z be the amplitude of this additional hopping, total Hamiltonian can be expressed as

$$\begin{aligned} H &= H_{vw} + H_z, \\ H_z &= \sum_{j=1}^{N} z\, c^{\dagger}_{\mathrm{A},j} c_{\mathrm{B},j+1} + \mathrm{h.c.}, \end{aligned} \quad (2)$$

and distribution of winding numbers in the parameter space of the system is given by

$$\nu = \begin{cases} 0, & |w+z| < v, \\ 1, & |w+z| > v \text{ and } w > z, \\ -1, & |w+z| > v \text{ and } w < z. \end{cases} \quad (3)$$

In another study, Pérez-González *et al* showed that an additional topological phase with $\nu = 2$ emerges in the presence of more than one further neighbor hopping terms[18]. Two distinct pairs of topological edge states are found to appear. In the presence of multiple further neighbor hopping terms, topological phases with higher winding numbers, say, up to $\nu = 4$ have been reported so far[19].

In this study we are going to show that a single additional hopping term is sufficient to produce the topological phases with any value of winding number as one wishes. Topological phases with higher values of winding numbers can be generated by systematically increasing the separation between the sites over which hopping is taken into account. Multiple pairs of edge states, consistent with the value of ν, are found to appear.

III. TOPOLOGICAL PHASES IN TERMS OF WINDING NUMBERS

In order to generate the topological phases with any values of winding numbers in the most simple way, two different types of eSSH models are introduced, however, both of them include a single further neighbor hopping term. Two different types of Hamiltonians are termed as 'A-B' and 'B-A' depending on the ordering of the sublattice sites and they are noted as $H^{\text{A-B}}_{z,n}$ and $H^{\text{B-A}}_{z,n}$, respectively, where $(n-1)$ is the number of intermediate primitive cells being covered under the hopping distance and z is the amplitude of the further neighbour hopping. In this nomenclature, Hamiltonian H_z in Eq. 2 can be specified as $H^{\text{A-B}}_{z,1}$. However, hopping only between different sublattices is allowed in this case. This type of hopping term preserves the particle-hole and inversion symmetries. Conservation of these symmetries means the preservation of chiral symmetry in addition. Now the topological properties of four different eSSH models will be studied in great details. Among them, two are of type 'B-A' and the remaining two are of type 'A-B'.

A. Topological phases for $H = H_{vw} + H^{\text{B-A}}_{z,2}$

Total Hamiltonian in this case is expressed as

$$H = H_{vw} + H^{\text{B-A}}_{z,2},$$

$$H^{\text{B-A}}_{z,2} = \sum_{j=1}^{N} z\, c^\dagger_{\text{B},j} c_{\text{A},j+2} + \text{h.c.}, \quad (4)$$

where the hopping term extends over one intermediate primitive cell, which is shown in Fig. 2. Under the

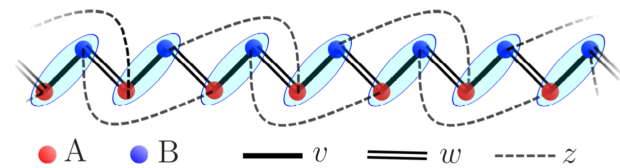

FIG. 2: Extended SSH model describing the hopping in $H^{\text{B-A}}_{z,2}$.

Fourier transformations,

$$c_{\text{A},j} = \frac{1}{\sqrt{N}} \sum_{\text{k}\in\text{BZ}} a_{\text{k}}\, e^{i\text{kj}},$$

$$c_{\text{B},j} = \frac{1}{\sqrt{N}} \sum_{\text{k}\in\text{BZ}} b_{\text{k}}\, e^{i\text{kj}},$$

where the summation extends over BZ, and assuming periodic boundary condition (PBC), the Hamiltonian in the k-space becomes

$$H = \sum_{\text{k}\in\text{BZ}} \Psi^\dagger_{\text{k}} H(\text{k}) \psi_{\text{k}},$$

for which $\Psi^\dagger_{\text{k}} = [a^\dagger_{\text{k}}\ b^\dagger_{\text{k}}]$, and $H(\text{k}) = \boldsymbol{g}(\text{k}) \cdot \boldsymbol{\sigma}$. Here, $\boldsymbol{\sigma} = (\sigma_x, \sigma_y, \sigma_z)$, are the Pauli matrices, and assuming the unit lattice parameter, $(a = 1)$,

$$\boldsymbol{g}(\text{k}) \equiv \begin{cases} g_x = v + w\cos(\text{k}) + z\cos(2\text{k}), \\ g_y = w\sin(\text{k}) + z\sin(2\text{k}), \\ g_z = 0. \end{cases}$$

It can be shown that $H(\text{k})$ satisfies the following transformation relations under the three different operators:

$$\begin{cases} \mathcal{T} H(\text{k}) \mathcal{T}^{-1} = H(-\text{k}), \\ \mathcal{P} H(\text{k}) \mathcal{P}^{-1} = -H(-\text{k}), \\ \sigma_z H(\text{k}) \sigma_z = -H(\text{k}), \end{cases}$$

where $\mathcal{T} = \mathcal{K}$, $\mathcal{P} = \mathcal{K}\sigma_z$ and $\mathcal{K}$ is the complex conjugation operator. These relations correspond to the conservation of time-reversal, particle-hole and chiral symmetries. As a consequence, inversion symmetry is preserved as $\sigma_x H(\text{k}) \sigma_x = H(-\text{k})$.

$\boldsymbol{g}(\text{k})$ can be spanned as a vector in the g_x-g_y complex plane, due to the conservation of chiral symmetry. As a result, the dispersion relation can be expressed as $E_\pm(\text{k}) = \pm|g(\text{k})|$, or, $E_\pm(\text{k}) = \pm\sqrt{v^2 + w^2 + z^2 + 2[vw\cos(\text{k}) + vz\cos(2\text{k}) + wz\cos(\text{k})]}$. Dispersions are symmetric around the energy, $E = 0$, since the Hamiltonian preserves particle-hole symmetry. Variation of dispersion relation, $E_+(\text{k})$, with $w/|v+z|$ for $v = 1$, $z = 1/2$ and $v = 3/4$, $z = 1$ are shown in Fig. 3 (a) and (b), respectively. The lower band, $E_-(\text{k})$ is not drawn. The figures in (a) and (b) are serving as prototype figures for $v/z > 1$ and $v/z < 1$, respectively. Dispersions comprise of one broad peak when $w/|v+z| \le 1$ for both the cases $v/z > 1$ and $v/z < 1$. Band gap vanishes at the BZ boundaries, $\text{k} = \pm\pi$ and $\text{k} = 0$, when $w = |v+z|$. As a result, ν is undefined at the point when $w = |v+z|$.

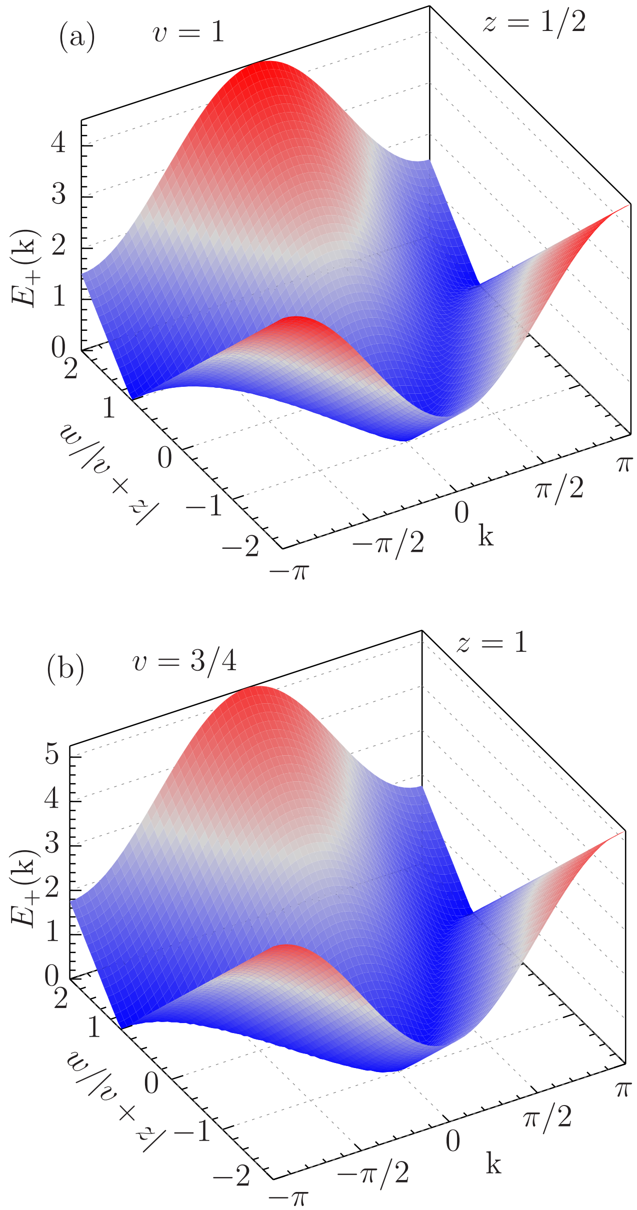

FIG. 3: Dispersion relation for $H = H_{vw} + H_{z,2}^{\text{A-B}}$ when $v/z > 1$, (a) and $v/z < 1$, (b).

B. Winding number, ν

Tip of the vector $\boldsymbol{g}(\mathrm{k})$ traces out closed loops in the g_x-g_y plane if k runs from $-\pi$ to π on the BZ. Winding number is defined to enumerate the number of closed loops around the origin of the plane. Mathematically it is expressed as

$$\nu = \frac{1}{2\pi}\int_{-\pi}^{\pi}\left[\hat{\boldsymbol{g}}(\mathrm{k}) \times \frac{\mathrm{d}}{\mathrm{dk}}\hat{\boldsymbol{g}}(\mathrm{k})\right]_z d\mathrm{k},$$

where $\hat{\boldsymbol{g}}(\mathrm{k}) = \boldsymbol{g}(\mathrm{k})/|\boldsymbol{g}(\mathrm{k})|$. Two distinct topological phases, with $\nu = 1, 2$ are found for this case in the parameter space as

$$\nu = \begin{cases} 1, & w > |z+v|, \\ 0, & w < |z+v|, \text{ and } v > z, \\ 2, & w < |z+v|, \text{ and } v < z, \end{cases} \tag{5}$$

and these are associated with a number of topological phase transitions.

For examples, when $v > z$, a transition takes place at $w = |v+z|$, separating trivial phase, $\nu = 0$ for $w < |v+z|$ and topological phase, $\nu = 1$ for $w > |v+z|$. Whereas, transition occurs at the same point between two topological phases when $v < z$. In this case, the phase for $w > |v+z|$ is marked by $\nu = 1$, while that for $w < |v+z|$ is identified by $\nu = 2$. In all cases transition takes place between the phases with energy gap, and obviously, gap closes at the transition point, $w = |v+z|$.

The parametric plot of winding diagrams in the g_x-g_y complex plane are shown in Fig. 4. Four figures are drawn for (a) $v = 0.5$, $w = 1.2$, $z = 0.3$, (b) $v = 0.5$, $w = 0.4$, $z = 0.3$, (c) $v = 0.3$, $w = 0.4$, $z = 0.5$, and (c) $v = 0.3$, $w = 0.4$, $z = 0.3$. Arrow head indicates the direction of move of the the vector $\boldsymbol{g}(\mathrm{k})$ for an infinitesimal increment of k. Tip of $\boldsymbol{g}(\mathrm{k})$ moves in counterclockwise direction over all the closed contours. The contours in (a) and (c) enclose the the origin, while that in (b) does not. On the other hand, contour in (d) passes over the origin. The curve passes around the origin once in (a) and twice in (c). Those figures serve as the prototype windings for the four different regions, $w > |v+z|$, $v > z$ for $\nu = 1$, $w < |v+z|$, $v > z$ for $\nu = 0$, $w < |v+z|$, $v < z$, for $\nu = 2$, and $w < |v+z|$, $v = z$. There is gap for the first three cases while the spectrum is gapless for the last.

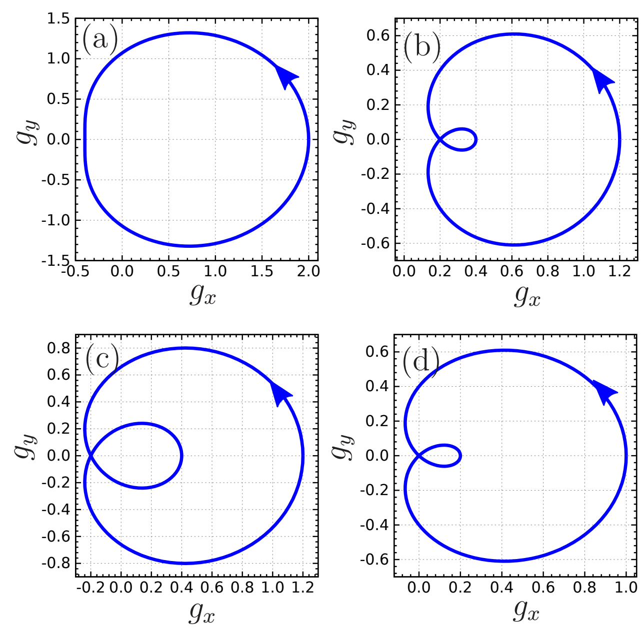

FIG. 4: Parametric winding diagrams in the g_x-g_y plane for the Hamiltonian, $H_{z,2}^{\text{B-A}}$. Four figures are drawn for (a) $v = 0.5$, $w = 1.2$, $z = 0.3$, (b) $v = 0.5$, $w = 0.4$, $z = 0.3$, (c) $v = 0.3$, $w = 0.4$, $z = 0.5$, and (c) $v = 0.3$, $w = 0.4$, $z = 0.3$.

Variation of bulk-edge state energies with respect to $w/|v+z|$ is shown in Fig. 5 as long as $w/|v+z| \leq \pm 2$. A single pair of zero energy edge states survives when $w > |v+z|$ as shown in (a). No edge state is there in this system when $w < |v+z|$ and and $v > z$. In contrast, zero energy edge states are always there when $w > |v+z|$ and $v < z$ which is shown in Fig. 5 (b). Actually, a single pair of zero energy edge states survives when $w > |v+z|$,

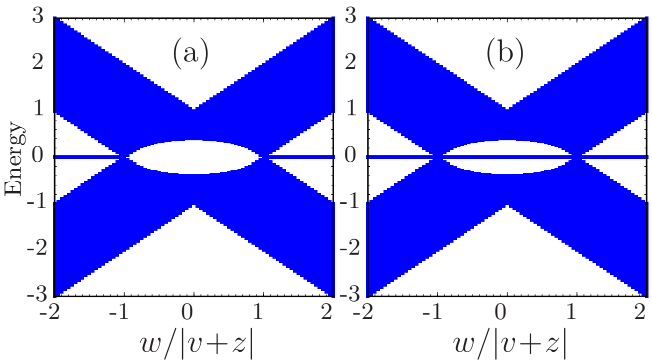

FIG. 5: Bulk and edge state energies for $H = H_{vw} + H^{\text{B-A}}_{z,2}$ when $v/z > 1$, (a) for $v = 0.7$, $z = 0.3$, and $v/z < 1$, (b) for $v = 0.3$, $z = 0.7$. Variation of energy with $w/|v{+}z|$ are shown for the lattice of 200 sites.

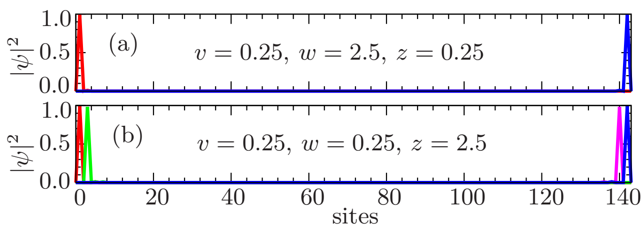

FIG. 6: Probability density of edge states for $H^{\text{B-A}}_{z,2}$: (a) for $v = 0.25$, $w = 2.5$, $z = 0.25$, one pair of edge states, (b) for $v = 0.25$, $w = 0.25$, $z = 2.5$, two pairs of edge states. Figures are drawn for the lattice of 142 sites.

and two pairs of edge states are there when $w < |v{+}z|$ and $v < z$. The figures are drawn for lattice of sites 200. All these results are consistent with the bulk-boundary correspondence rule.

In order to confirm the presence of zero energy edge states, probability density of those states are drawn in Fig. 6 for the lattice of 142 sites. Two figures are drawn for two distinct topological phases. In the upper panel (a), probability densities of two distinct edge states with $E = 0$ are shown when $v = 0.25$, $w = 2.5$, $z = 0.25$, as these values confirm to the conditions, $w > |v{+}z|$. Probability density of one edge state exhibits sharp peak at site $m = 1$ and another one at site $m = 142$. This corresponds to the topological phase with $\nu = 1$. On the other hand, for $w < |v{+}z|$ and $v < z$, probability densities of four distinct edge states with $E = 0$ are shown in the lower panel (b) when $v = 0.25$, $w = 0.25$, $z = 2.5$, as these values are in accordance to the last conditions. Probability density of four orthogonal edge states exhibit sharp peak at sites $m = 1$, $m = 3$, $m = 140$, and $m = 142$. It indicates that zero energy states near the left edge are localized on the A sublattice, while those close to the right edge are localized on the B sublattice. This result is in accordance to the topological phase with $\nu = 2$.

An extensive phase diagram of the total Hamiltonian including $H^{\text{B-A}}_{z,2}$ is shown in Fig 7. Here contour plot for ν is drawn in the v-$w/|v+z|$ space. Presence of two distinct topological phases, $\nu = 1$ and 2 along with the trivial phase, $\nu = 0$ are shown in green, blue and red, respectively. The horizontal line is drawn at $v = 1$ or $v/z = 1$ since this diagram is drawn for $v + z = 2$. The line segment within the points $w/(v+z) = \pm 1$ separates the trivial phase from the topological phase with $\nu = 2$. Hence phase transition occurs around this segment. Another topological phase with $\nu = 1$ appears beyond the two vertical lines drawn at $w/(v+z) = \pm 1$. They separate topological phases with $\nu = 1$ and 2 when $v/z < 1$ and topological ($\nu = 1$) and trivial phase when $v/z > 1$. So the system undergoes phase transition around those straight lines. Band gap vanishes over those lines as well as on the line segment.

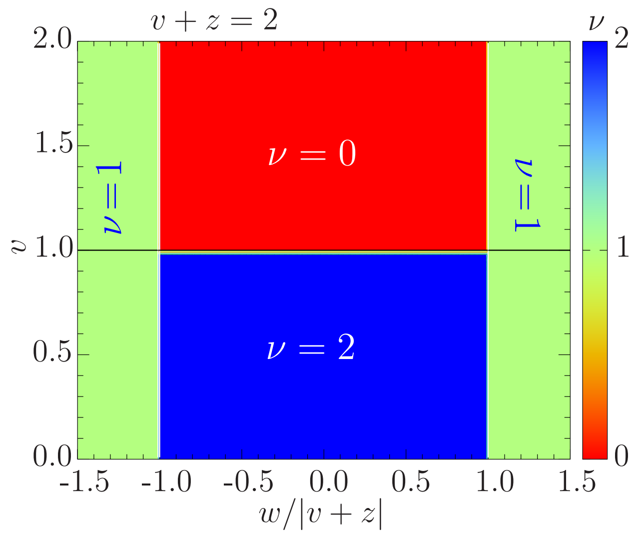

FIG. 7: Topological phase diagram for the Hamiltonian, $H^{\text{B-A}}_{z,2}$. Trivial phase is shown by red ($\nu = 0$) while two distinct topological phases are shown by green ($\nu = 1$) and blue ($\nu = 2$). This diagram is drawn for $v + z = 2$. The horizontal line indicates the value $v = 1$ or $v/z = 1$.

C. Quenched dynamics in the presence of nonlinear terms

Now the effect of nonlinearity on the topological phase will be studied following the method developed by Ezawa[33]. Schrödinger equation for a Hamiltonian matrix, M, spanned on a lattice composed of L sites can be written as ($\hbar = 1$),

$$i\,\frac{\partial \psi_l}{\partial t} + \sum_{m=1}^{L} M_{lm}\,\psi_l = 0. \tag{6}$$

It actually comprises L coupled linear equations and governs the time evolution of the system where M_{lm} is recognized as the element of hopping matrix in case of tight-binding model. This system hosts the topological as well as trivial phases for different parameter regime.

The eigenvalue equation for the hopping matrix, M is written as

$$M\bar{\phi}_q = E_q\bar{\phi}_q,\ 1 \le q \le L, \tag{7}$$

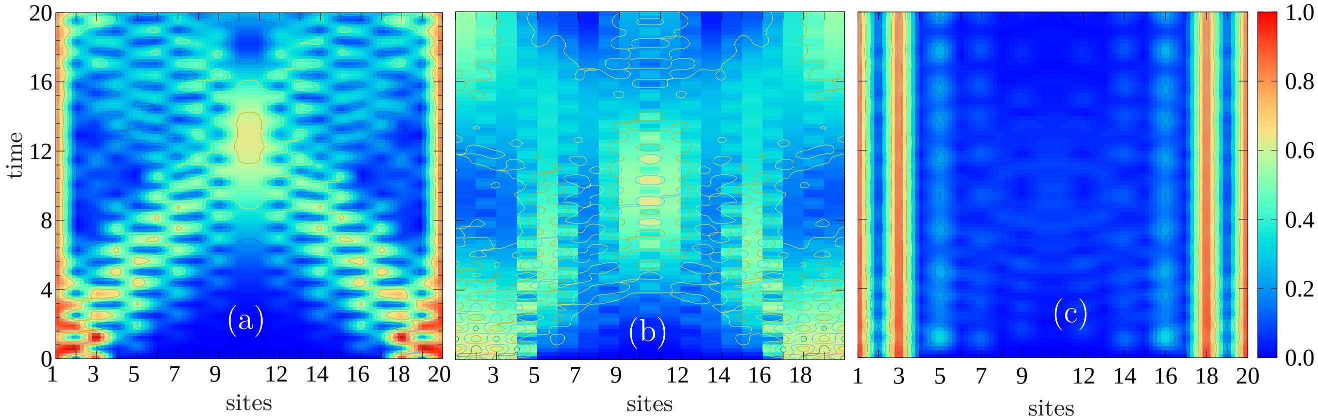

FIG. 8: Quench dynamics for $H^{\text{B-A}}_{z,2}$ when $\zeta = 0.5$, (a) for $v = 0.25$, $w = 2.5$, $z = 0.25$, (b) for $v = 2.5$, $w = 0.25$, $z = 0.25$, (c) for $v = 0.25$, $w = 0.25$, $z = 2.5$. Figures are drawn for lattice with 20 sites.

where q serves as the quantum index. Hence, time evolution of the model is governed by the solution of Eq. 6 as

$$\bar{\phi}_q(t) = e^{-itE_q}\,\bar{\phi}_q(t), \tag{8}$$

since the Schrödinger equation eventually turns into a set of decoupled equations

$$i\,\frac{\partial\bar{\phi}_q}{\partial t} + \sum_{m=1}^{L} M_{lm}\,\bar{\phi}_q = 0. \tag{9}$$

The variation of energies E_q with $w/|v+z|$ for two different topological phases have been shown in the Fig. 5, when the hopping matrix is constituted for the Hamiltonian defined in Eq. 4 for the lattice of sites $L = 200$. Topological phases are always protected by the zero energy edge states by virtue of particle-hole symmetry of the system. As a result, no time evolution of those localized states is permissible according to the Eq. 8. In light of this fact, time evolution of the edge states in the presence of additional nonlinear term will be studied.

The Schrödinger equation in the presence of nonlinear term for the one-dimensional tight-binding model of hopping matrix M_{lm} is defined by

$$i\frac{\partial\psi_l}{\partial t} + \sum_{m}^{L} M_{lm}\psi_l + \zeta|\psi_l|^2\psi_l = 0, \tag{10}$$

where the effect of nonlinearity is controlled by the parameter ζ. Explicit form of the set of coupled nonlinear first order differential equation for finite chain of L sites and for the Hamiltonian defined in Eq. 4 with open boundary condition (OBC) is given by

$$\begin{aligned} i\,\frac{\partial\psi_{2j-1}}{\partial t} &= v(\psi_{2j}-\psi_{2j-1}) + w(\psi_{2j-2}-\psi_{2j-1}) \\ &\quad + z(\psi_{2j-4}-\psi_{2j-1}) - \zeta|\psi_{2j-1}|^2\psi_{2j-1}, \\ \vdots \quad &= \qquad\qquad \vdots \\ i\,\frac{\partial\psi_{2j}}{\partial t} &= w(\psi_{2j+1}-\psi_{2j}) + v(\psi_{2j-1}-\psi_{2j}) \\ &\quad + z(\psi_{2j+3}-\psi_{2j}) - \zeta|\psi_{2j}|^2\psi_{2j}, \end{aligned} \tag{11}$$

where j denotes the cell index which ultimately generates L number of coupled equations each one for every site. So, $j = 1, 2, 3, \cdots, N/2$. Differential equations for odd and even sites are different since the translational symmetry of one lattice unit is broken.

The fate of the topological state when $\zeta \neq 0$ will be studied in terms of the time evolution of the nonlinear system by imposing an initial condition,

$$\psi_l(t) = \delta_{l,m} \quad \text{when} \;\; t = 0.$$

It means a delta-function like pulse at the m-th site is given initially. Henceforth dynamics of the resulting nonlinear system will be examined by maintaining the conservation rule imposed by the equation,

$$\sum_{l=1}^{L} |\psi_l(t)|^2 = \text{constant}. \tag{12}$$

Value of the constant may be fixed depending on the choice of the initial conditions. The initial conditions in turn depend on the value of winding number for a particular topological phase. It is shown that topological phase defined in the linear system is robust against the introduction of the nonlinear term as long as $\zeta < 1$, as a result, quenching of the edge states are observed.

As the general solution of the Eq. 10 can be expanded as

$$\psi_l(t) = \sum_q c_q(t)\bar{\phi}_q(t),$$

the initial state can be expressed as

$$\psi_l(0) = \delta_{l,m} = \sum_q c_q\bar{\phi}_q(0). \tag{13}$$

The topological phase of the linear system is always protected by the presence of zero energy edge (localized) states. So keeping in mind the position of edge states, initial condition is imposed either by $l = 1$ or $l = L$, when $\nu = 1$. Here $l = 1$ ($l = L$) denotes the leftmost (rightmost) site of the lattice. Now for $l = 1$, initial condition turns out as $\psi_l(0) = \delta_{l,1}$. Right hand side of the Eq. 13 may be simplified by labeling the zero energy state by $\bar{\phi}_1$ with $E_1 = 0$ in Eq. 7. So, at $t = 0$,

$$\psi_1(0) = c_1\bar{\phi}_1(0). \tag{14}$$

As $E_1 = 0$, $\bar{\phi}_q(t) = \bar{\phi}_q(0)$, which leads to the fact that

$$\psi_1(t) = c_1\bar{\phi}_1(0).$$

It means no time evolution of the edge states is there or in other words a non-zero probability amplitude at the edge site remains at any time. It corresponds to the quenching of the edge states. No such quenching is possible for the bulk states by virtue of their non-zero energy, ($E_q \neq 0$).

In contrast, zero-energy localized states are absent in the trivial phase, and all the states are found to extend within the bulk. As a result, quenching dynamics of edge states may serve as an alternative numerical tool to distinguish the topological and trivial phases by investigating the effect of nonlinear component on the initial condition. At the same time, investigation of quench dynamics for systems under PBC is meaningless, since no edge state is there.

Quenching of edge states for the nonlinear system is shown in Fig. 8, by solving the set of Eq. 11, for $L = 20$ when $\zeta = 0.5$. Contour plot for the time evolution of the absolute value of complex amplitude, $|\psi_l(t)|$, is drawn for every site, $l = 1, 2, 3, \cdots, 20$, which is shown along the horizontal axis. Three contour plots are shown (a) for $v = 0.25$, $w = 2.5$, $z = 0.25$, (b) for $v = 2.5$, $w = 0.25$, $z = 0.25$, (c) for $v = 0.25$, $w = 0.25$, $z = 2.5$, where (b) indicates trivial phase while (a) and (c) for the topological phases of $\nu = 1$ and $\nu = 2$. Initial condition is set by $\psi_l(0) = \delta_{l,m}$, where $m = 1, 3, 18, 20$. Which means the initial pulse is given only at those sites. As a result, conservation rule follows the relation, $\sum_{l=1}^{L} |\psi_l(t)|^2 = 4$.

Time evolution is explored for the span, $0 \leq t \leq 20$, which is plotted along the vertical axis. The diagram clearly indicates that probability amplitudes for $l = 1, 20$, *i. e.*, $|\psi_1(t)|$ and $|\psi_{20}(t)|$ survive with time in (a). So the edge states bound to the topological phase with $\nu = 1$ exhibit their quenching. No such quenching is found for the trivial phase as shown in (b). Quenching of four edge states, $|\psi_l(t)|$, $l = 1, 3, 18, 20$ are found in (c) which correspond to the topological phase with $\nu = 2$. So for the lattice with L sites, quenching are found for the amplitude with sites $l = 1, 3, L-2, L$. It is true that the diagram exhibiting the quenching of edge states will be different if the initial conditions are made different from this set. However, this particular choice of initial conditions is considered from the previous knowledge of locations of the peaks of probability density of edge states as shown in Fig. 6. Hence the quench dynamics provide another route for distinguishing topological and trivial phases for a system.

D. Topological phases for $H = H_{vw} + H_{z,2}^{\text{A-B}}$

Total Hamiltonian in this case is

$$\begin{aligned} H &= H_{vw} + H_{z,2}^{\text{A-B}}, \\ H_{z,2}^{\text{A-B}} &= \sum_{j=1}^{N} z\, c_{\text{A},j}^{\dagger} c_{\text{B},j+2} + \text{h.c.}, \end{aligned} \tag{15}$$

where the hopping term once again extends over one intermediate primitive cell, which is shown in Fig. 9. As a result,

$$\boldsymbol{g}(\text{k}) \equiv \begin{cases} g_x = v + w\cos(\text{k}) + z\cos(2\text{k}), \\ g_y = w\sin(\text{k}) - z\sin(2\text{k}), \\ g_z = 0. \end{cases}$$

Dispersion relation in this case is $E_{\pm}(\text{k}) = \pm\sqrt{v^2 + w^2 + z^2 + 2[vw\cos(\text{k}) + vz\cos(2\text{k}) + wz\cos(3\text{k})]}$.

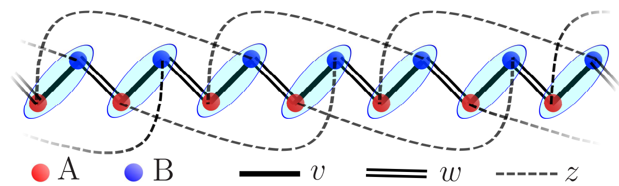

FIG. 9: Extended SSH model describing the hopping in $H_{z,2}^{\text{A-B}}$.

Variation of dispersion relation, $E_{+}(\text{k})$, with $w/|v + z|$ for $v = 1$, $z = 1/2$ and $v = 1/2$, $z = 1$ are shown in Fig. 10 (a) and (b), respectively. Those are serving as prototype figures for $v/z > 1$ and $v/z < 1$, respectively. Dispersions comprise of three peaks for any values of the parameters, v, w and z. Like the previous case, band gap vanishes at $\text{k} = \pm\pi$, and $\text{k} = 0$, when $w = |v + z|$, for both the cases $v/z > 1$ and $v/z < 1$. As a result, ν is undefined again at the point when $w = |v + z|$. But in the region, $w < |v + z|$, for $v < z$, the system undergoes an additional phase transition at the point defined by the set of equations, $E_{\pm}(\text{k}) = 0$, and $\frac{dE_{\pm}(\text{k})}{d\text{k}} = 0$, which will be discussed later.

Also, in this case, two different topological phases appear in the parameter space as given below which are separated by phase transition lines.

$$\nu = \begin{cases} 1, & w > |z + v|, \\ 0, & w < |z + v|, \text{ and } v > z, \\ -2, 0 & w < |z + v|, \text{ and } v < z. \end{cases} \tag{16}$$

Topological phase with $\nu = 1$ exists as along as the relation $w > |z + v|$ holds irrespective of individual values of v and z. Another nontrivial phase with $\nu = -2$ appears in a limited region for $w < |z + v|$ and $v < z$, separated by trivial phase. The equation of phase transition line can be obtained by satisfying the conditions, $E_{\pm}(\text{k}) = 0$, and $\frac{dE_{\pm}(\text{k})}{d\text{k}} = 0$. Anyway, this model hosts the new topological phase with $\nu = -2$.

The parametric plot of winding by the tip of the vector, $\boldsymbol{g}(\text{k})$ in the g_x-g_y complex plane is shown in Fig. 11. Four figures are drawn for (a) $v = 0.5$, $w = 1.2$, $z = 0.3$, (b)

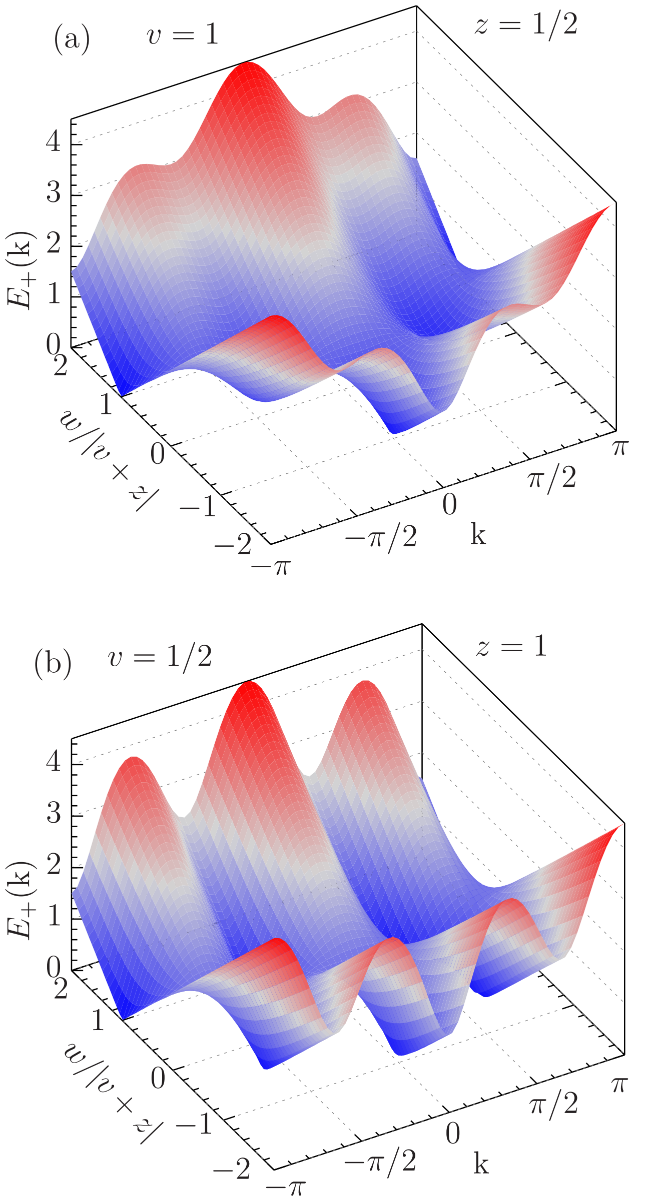

FIG. 10: Dispersion relation for $H^{\text{A-B}}_{z,2}$ when $v/z > 1$, (a) and $v/z < 1$, (b).

$v = 0.5$, $w = 0.5$, $z = 0.3$, (c) $v = 0.3$, $w = 0.2$, $z = 0.5$, and (d) $v = 0.45$, $w = 0.6$, $z = 0.5$. Those figures serve as the prototype contours for the four different regions, $w > |v + z|$, for $\nu = 1$, $w < |v + z|$, $v > z$ for $\nu = 0$, $w < |v + z|$, $v < z$, for $\nu = -2$ and $\nu = 0$. $\boldsymbol{g}(\mathrm{k})$ traces the closed contour in counter clockwise direction for (a) and (b) while it is clockwise for (c) and (d). Curve encloses the origin once in (a) and twice in (c) but in opposite direction which corresponds to winding numbers of opposite sign. Nonzero band gap is there for all the cases.

Variation of bulk-edge state energies with respect to $w/|v+z|$ is shown in Fig. 12 for the regime $-2 \leq (w/|v+z|) \leq 2$. A single pair of zero energy edge states is there when $w > |v + z|$ as shown in (a). No edge state is there in this system when $w < |v+z|$ and and $v > z$. However, two pairs of zero energy edge states appear in a region around the point $w/|v + z| = 0$ when $w < |v + z|$ and

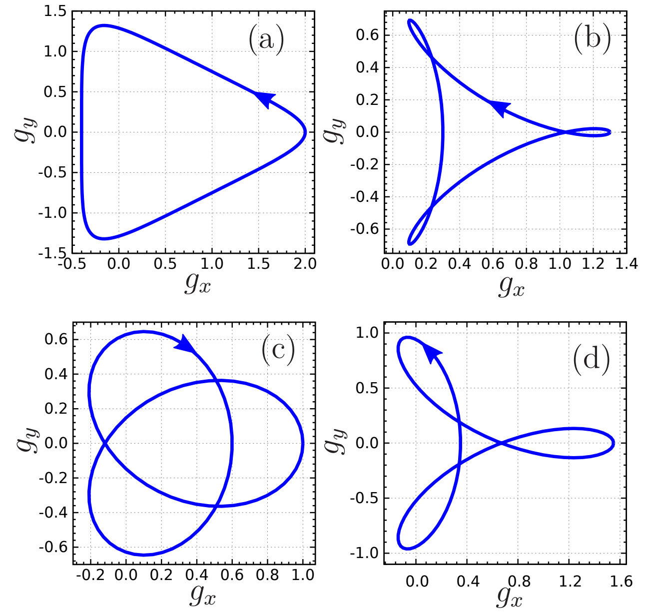

FIG. 11: Parametric winding diagrams in the g_x-g_y plane for the Hamiltonian, $H^{\text{A-B}}_{z,2}$. Four figures are drawn for (a) $v = 0.5$, $w = 1.2$, $z = 0.3$, (b) $v = 0.5$, $w = 0.5$, $z = 0.3$, (c) $v = 0.3$, $w = 0.2$, $z = 0.5$, and (c) $v = 0.45$, $w = 0.6$, $z = 0.5$.

$v < z$ which is shown in Fig. 12 (b). This particular region is surrounded by a trivial phase as long as $-1 \leq (w/|v + z|) \leq 1$. The figures are drawn for lattice of sites 200, and the results confirm the existence of edge states in the topological phases.

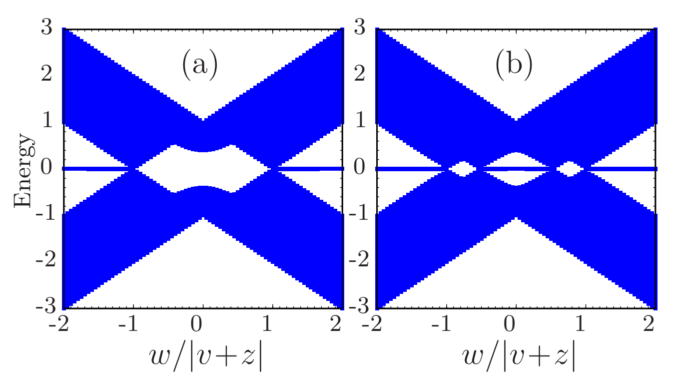

FIG. 12: Bulk and edge state energies for $H = H_{vw} + H^{\text{A-B}}_{z,2}$ when $v/z > 1$, (a) for $v = 0.7$, $z = 0.3$, and $v/z < 1$, (b) for $v = 0.3$, $z = 0.7$.

To make sure the presence of zero energy edge states, probability densities of those states are drawn in Fig. 13 for the lattice of 150 sites. Two figures are drawn for two distinct topological phases. In the upper panel (a), probability densities of two distinct edge states with $E = 0$ are shown when $v = 0.25$, $w = 2.5$, $z = 0.25$. Those values are selected for satisfying the conditions, $w > |v + z|$. Probability density of one edge state exhibits sharp peak at site $m = 1$ and another one at site $m = 150$. This corresponds to the topological phase with $\nu = 1$. On the other hand, for $w < |v + z|$ and $v < z$, probability density of four distinct zero energy edge states are shown in the lower panel (b) when $v = 0.25$, $w = 0.25$, $z = 2.5$.

Probability density of four orthogonal edge states exhibits sharp peak at sites $m = 2$, $m = 4$, $m = 147$, and $m = 149$. In this case zero energy states close to the left edge are localized on the B sublattice, while those close to the right edge are localized on the A sublattice. The difference on localization with respect to the previous case attributes to the change in the sign of the winding number, as the new topological phase of $\nu = -2$, appears with opposite sign with respect to previous case.

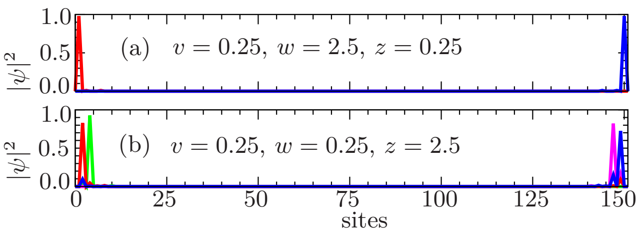

FIG. 13: Probability density of edge states for $H = H_{vw} + H_{z,2}^{\text{A-B}}$: (a) for $v = 0.25$, $w = 2.5$, $z = 0.25$, one pair of edge state, (b) for $v = 0.25$, $w = 0.25$, $z = 2.5$, two pairs of edge states. Figures are drawn for the lattice of 150 sites.

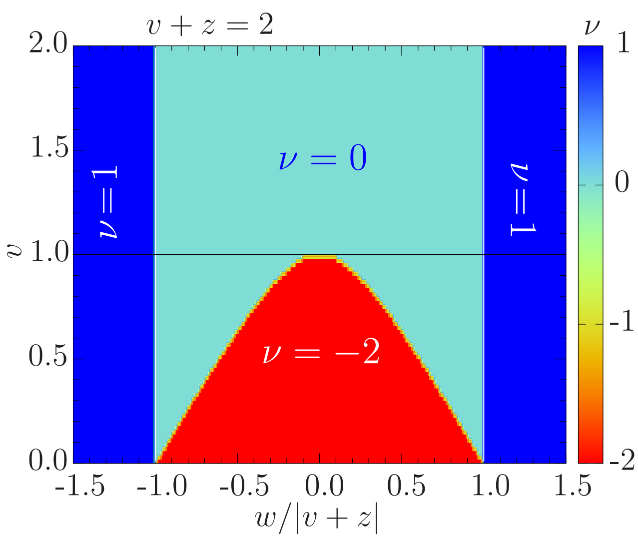

FIG. 14: Topological phase diagram for the Hamiltonian, $H = H_{vw} + H_{z,2}^{\text{A-B}}$. Two distinct topological phases are shown by blue ($\nu = 1$) and red ($\nu = -2$). The remaining portion is trivial ($\nu = 0$). This diagram is drawn for $v + z = 2$. The horizontal line indicates the value $v = 1$ or $v/z = 1$.

A comprehensive phase diagram for this model is shown in Fig 14 where contour plot for ν is drawn in the v-$w/|v + z|$ space. Variation of the parameters is made by maintaining the constraint $v + z = 2$. Existence of two different topological phases, $\nu = 1$ and -2, along with the trivial phase, $\nu = 0$ are shown in three different colours. The horizontal line is drawn at $v/z = 1$, above which topological phase with $\nu = -2$ does not survive. This phase exists over the line segment, $-1 \leq w/(v+z) \leq +1$, when $v = 0$. However the length of this segment reduces symmetrically around $w/(v + z) = 0$ and vanishes at the point $v = z$. The boundary lines of these phases can be obtained by simultaneously solving the Eqs. $E_{\pm}(\text{k}) = 0$, and $\frac{dE_{\pm}(\text{k})}{d\text{k}} = 0$. As a result, the transition lines are given by the two solutions of quadratic equation, $v^2+w^2+z^2+2\{vwp+vz(2p^2-1)+wzp(4p^2-3)\} = 0$, where $p = \cos^{-1}\left(\frac{-vz\pm\sqrt{v^2z^2-3w^2z(v-3z)}}{6wz}\right)$, along with the constraint, $v + z = 2$. These curved lines are symmetric around the straight line $w/(v + z) = 0$ and meet at the point, $w/(v + z) = 0$, $v = 1$. Another topological phase with $\nu = 1$ appears beyond the two vertical lines drawn at $w/(v + z) = \pm 1$. They separate topological phase with $\nu = 1$ from the trivial phase. So the system undergoes phase transition around those straight lines.

As the quenching of edge states provides their exact location more clearly, dynamics of the edge states in the presence of nonlinear terms for the topological phases of this model will be discussed. The set of coupled nonlinear first order differential equation for finite chain of L sites and for the Hamiltonian defined in Eq. 15 with OBC is explicitly given by

$$\begin{aligned} i\,\frac{\partial \psi_{2j-1}}{\partial t} &= v(\psi_{2j} - \psi_{2j-1}) + w(\psi_{2j-2} - \psi_{2j-1}) \\ &\quad + z(\psi_{2j+4} - \psi_{2j-1}) - \zeta|\psi_{2j-1}|^2\psi_{2j-1}, \\ \vdots \quad &= \quad \vdots \\ i\,\frac{\partial \psi_{2j}}{\partial t} &= w(\psi_{2j+1} - \psi_{2j}) + v(\psi_{2j-1} - \psi_{2j}) \\ &\quad + z(\psi_{2j-5} - \psi_{2j}) - \zeta|\psi_{2j}|^2\psi_{2j}. \end{aligned} \tag{17}$$

Quenching of edge states for the nonlinear system is shown in Fig. 15, by solving the set of Eq. 17, for $L = 20$, when $\zeta = 0.5$. Contour plot for the time evolution of $|\psi_l(t)|$, is drawn for every site which is shown along the horizontal axis. Three contour plots are shown (a) for $v = 0.25$, $w = 2.5$, $z = 0.25$, (b) for $v = 2.5$, $w = 0.25$, $z = 0.25$, (c) for $v = 0.25$, $w = 0.25$, $z = 2.5$, where (b) indicates trivial phase as before while (a) and (c) for the topological phases of $\nu = 1$ and $\nu = -2$, respectively. In this case, initial condition is set by $\psi_l(0) = \delta_{l,m}$, where $m = 2, 4, 17, 19$. As a result, conservation rule follows the same equation as before, $\sum_{l=1}^{L} |\psi_l(t)|^2 = 4$.

Evolution of the system is explored for the time span, $0 \leq t \leq 20$, where the time is plotted along the vertical axis. The diagram in (a) clearly indicates that probability amplitudes for $l = 1, 20$, *i. e.*, $|\psi_1(t)|$ and $|\psi_{20}(t)|$ survive with time. So the edge states bound to the topological phase with $\nu = 1$ exhibit their quenching. No such quenching is found for the trivial phase as shown in (b). Those results are similar to the previous case, although the respective figures are qualitatively different. Quenching of four edge states, $|\psi_l(t)|$, when $l = 2, 4, 17, 19$ are found in (c) which correspond to the topological phase with $\nu = -2$. In contrast to this result, quenching of four edge states, for $l = 1, 3, 18, 20$ are found when $\nu = 2$, as discussed in the previous model. It means quenching over A and B sublattices interchange their edges with the change in sign of ν. Thus, quenching are found for the amplitude on sites, $l = 2, 4, L-3, L-1$, for any arbitrary length of lattice.

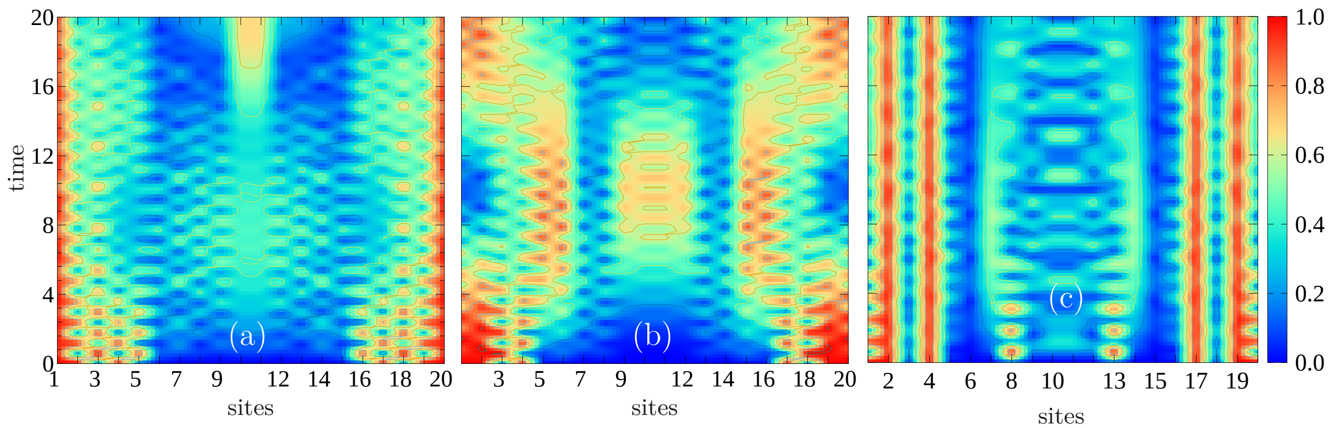

FIG. 15: Quench dynamics for $H = H_{vw} + H_{z,2}^{\text{A-B}}$ when $\zeta = 0.5$, (a) for $v = 0.25$, $w = 2.5$, $z = 0.25$, (b) for $v = 2.5$, $w = 0.25$, $z = 0.25$, (c) for $v = 0.25$, $w = 0.25$, $z = 2.5$. Figures are drawn for lattice with 20 sites.

E. Topological phases for $H = H_{vw} + H_{z,3}^{\text{B-A}}$

Now the total Hamiltonian is

$$\begin{aligned} H &= H_{vw} + H_{z,3}^{\text{B-A}}, \\ H_{z,3}^{\text{B-A}} &= \sum_{j=1}^{N} z\, c_{\text{B},j}^{\dagger} c_{\text{A},j+3} + \text{h.c.}, \end{aligned} \tag{18}$$

where the hopping term extends over two intermediate primitive cell, which is shown in Fig. 16. In this model

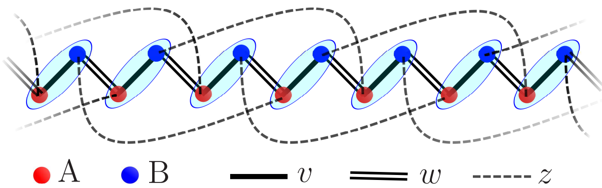

FIG. 16: Extended SSH model describing the hopping in $H_{z,3}^{\text{B-A}}$.

every cell is connected to the third NN cell by the hopping parameter z. The $\boldsymbol{g}(\text{k})$ vector assumes the form,

$$\boldsymbol{g}(\text{k}) \equiv \begin{cases} g_x = v + w\cos(\text{k}) + z\cos(3\text{k}), \\ g_y = w\sin(\text{k}) + z\sin(3\text{k}), \\ g_z = 0. \end{cases}$$

Dispersion relation in this case is $E_{\pm}(\text{k}) = \pm\sqrt{v^2 + w^2 + z^2 + 2[vw\cos(\text{k}) + vz\cos(3\text{k}) + wz\cos(2\text{k})]}$. Variation of dispersion relation, $E_{+}(\text{k})$, with $v/|w+z|$ for $w = 1$, $z = 1/2$ and $w = 1/2$, $z = 1$ are shown in Fig. 17 (a) and (b), respectively. Those are serving as prototype figures for $w > z$ and $w < z$, respectively. Dispersions comprise of three broad peaks when $v/|w + z| \le 1$, for both the cases $w/z > 1$ and $w/z < 1$. Band gap vanishes at the BZ boundaries, $\text{k} = \pm\pi$, and $\text{k} = 0$ when $v = |w+z|$. As a result, ν is undefined at the point when $v = |w + z|$. The dispersions plotted in Figs. 10 and 17 look alike although they are different in a sense that they are plotted with respect to different parameters, say, $w/|v + z|$ in Fig. 10 and $v/|w + z|$ in Fig. 17. This similarity attributes to the fact that dispersions for the Hamiltonians in Eqs. 15 and 18 are interchangeable upon interchange of v and w.

In this case also two different types of topological phases with $\nu = 1$ and 3 appear in the parameter space as given below and they are separated by phase transition lines.

$$\nu = \begin{cases} 0, & v > |w + z|, \\ 1, & v < |w + z|, \text{ and } w > z, \\ 3, 1, & v < |w + z|, \text{ and } w < z. \end{cases} \tag{19}$$

The system is trivial as long as $v > |w + z|$, irrespective of the values of w and z. Topological phase with $\nu = 1$ exists when the relations $v < |w + z|$ and $w > z$ do hold. Another nontrivial phase with $\nu = 3$ appears in a limited region for $v < |w+z|$ and $w < z$, separated by the topological phase with $\nu = 1$. It means the phase with $\nu = 1$ emerges for $v < |w + z|$ for both $w > z$ and $w < z$. The equation of phase transition lines can be obtained by satisfying the conditions, $E_{\pm}(\text{k}) = 0$, and $\frac{dE_{\pm}(\text{k})}{d\text{k}} = 0$. So, this model hosts the new topological phase with $\nu = 3$.

The parametric plot of winding by the tip of the vector, $\boldsymbol{g}(\text{k})$ in the g_x-g_y complex plane are shown in Fig. 18. Four figures are drawn for (a) $v = 1.1$, $w = 0.6$, $z = 0.4$, (b) $v = 0.7$, $w = 0.6$, $z = 0.4$, (c) $v = 0.2$, $w = 0.4$, $z = 0.6$, and (d) $v = 0.7$, $w = 0.4$, $z = 0.6$. All the curves traverse in the counter clockwise direction, as a result of which, all the winding numbers are positive. Those figures serve as the prototype contours for the four different regions, $v > |w+z|$, for $\nu = 0$, $v < |w+z|$, $w > z$ for $\nu = 1$, $v < |w + z|$, $w < z$, for $\nu = 3$ and $\nu = 1$. $\boldsymbol{g}(\text{k})$. Nonzero band gap is there for all the cases.

Variation of bulk-edge state energies with respect to $v/|w+z|$ is shown in Fig. 19 for the regime $-2 \le (v/|w+z|) \le 2$. No zero energy edge states is there when $v > |w + z|$ as shown in (a). Single pair of edge state is there in this system when $v < |w+z|$ and and $w > z$. However, three pairs of zero energy edge states appear in a region

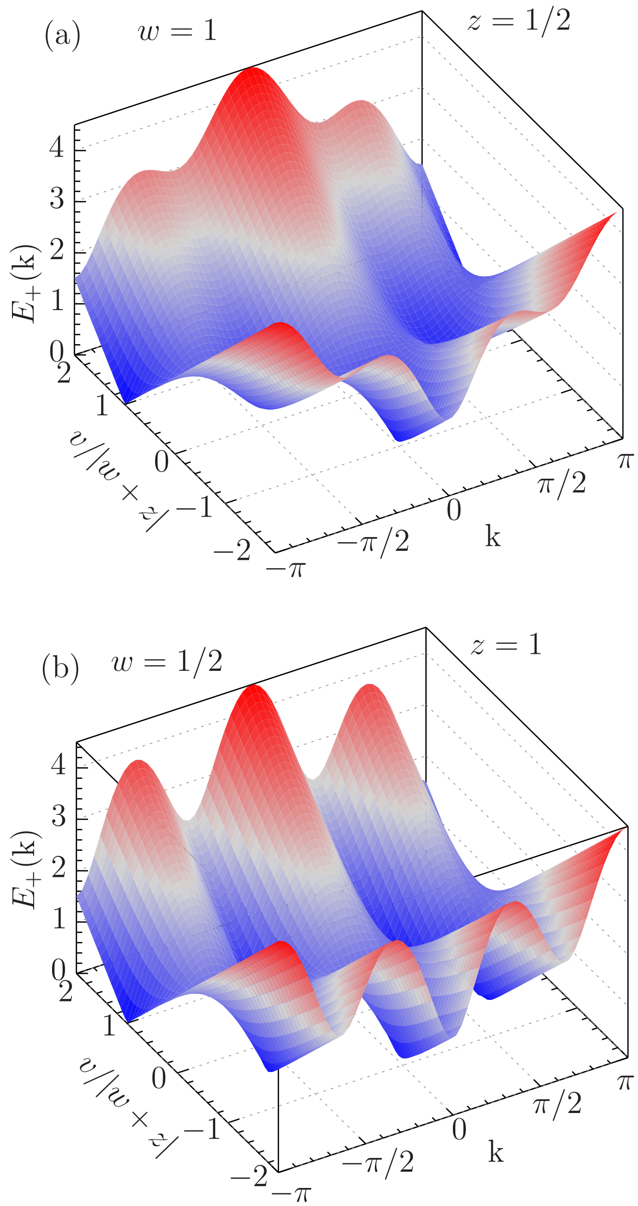

FIG. 17: Dispersion relation for $H_{z,3}^{\text{B-A}}$ when $w/z > 1$, (a) and $w/z < 1$, (b).

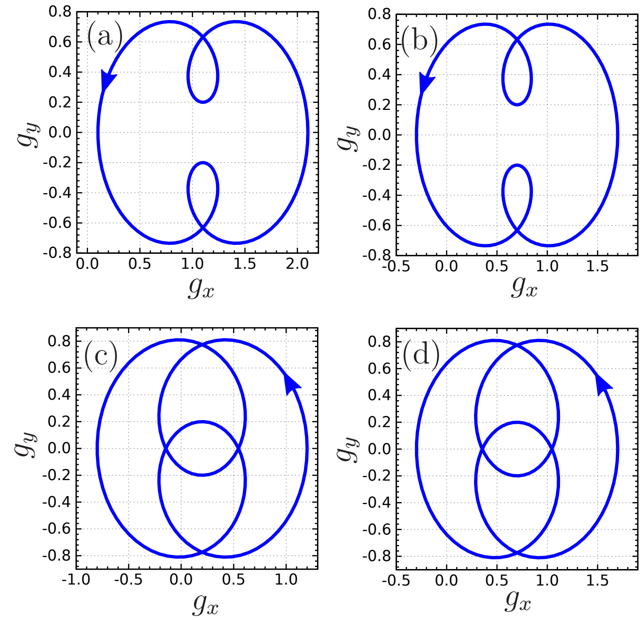

FIG. 18: Parametric winding diagrams in the g_x-g_y plane for the Hamiltonian, $H_{z,3}^{\text{B-A}}$. Four figures are drawn for (a) $v = 1.1$, $w = 0.6$, $z = 0.4$, (b) $v = 0.7$, $w = 0.6$, $z = 0.4$, (c) $v = 0.2$, $w = 0.4$, $z = 0.6$, and (c) $v = 0.7$, $w = 0.4$, $z = 0.6$.

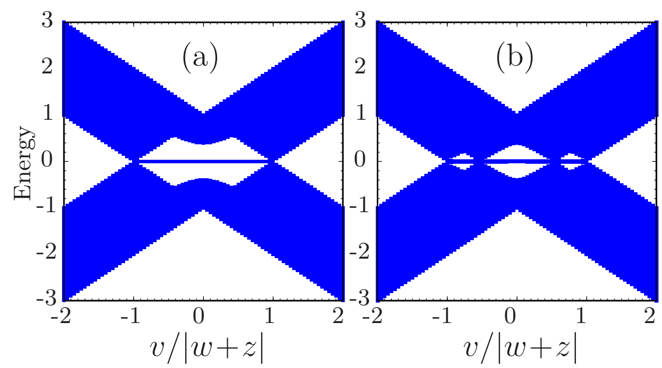

FIG. 19: Edge states for $H = H_{vw} + H_{z,3}^{\text{B-A}}$ when $w/z > 1$, (a) for $w = 0.7$, $z = 0.3$, and $w/z < 1$, (b) for $w = 0.3$, $z = 0.7$.

around the point $v/|w+z| = 0$ when $v < |w+z|$ and $w < z$ which is shown in Fig. 19 (b). This particular region is surrounded by a single pair of edge states as long as $-1 \leq (v/|w+z|) \leq 1$. The figures are drawn for lattice of sites 200, and the results confirm the existence of edge states in the topological phases.

In order to confirm the existence of zero energy edge states, probability densities of those states are drawn in Fig. 20 for the lattice of 200 sites. Two figures are drawn for two distinct topological phases. In the upper panel (a), probability densities of two distinct edge states with $E = 0$ are shown when $v = 0.25$, $w = 2.5$, $z = 0.25$. Those values are selected for satisfying the conditions, $v < |w+z|$ and $w > z$. Probability density of one edge state exhibits sharp peak at site $m = 1$ and another one at site $m = 200$. This corresponds to the topological phase with $\nu = 1$. On the other hand, for $v < |w+z|$ and $w < z$, probability density of four distinct zero energy edge states are shown in the lower panel (b) when $v = 0.25$, $w = 0.25$, $z = 2.5$. Probability density of six orthonormal edge states exhibit sharp peak at sites $m = 1, 3, 5, 196, 198$ and 200. This result is in accordance to the topological phase of $\nu = 3$. Here localization of zero energy states are found on A sublattice near left edge and B sublattice near right edge.

A rigorous phase diagram for this model is shown in Fig 21 where contour plot for ν is drawn in the w-$v/|w+z|$ space. Variation of the parameters is made by maintaining the constraint $w + z = 2$. Existence of two different topological phases, $\nu = 1$ and 3 along with the trivial phase, $\nu = 0$ are shown in yellow, blue and red. The horizontal line is drawn at $w/z = 1$, above which topological phase with $\nu = 3$ does not survive. This phase exists over the line segment, $-1 \leq v/(w+z) \leq +1$, when $w = 0$. However the length of this segment reduces symmetrically around $v/(w+z) = 0$ and vanishes at the point $w = z$. The boundary lines of separation of those phases can be obtained as before by solving

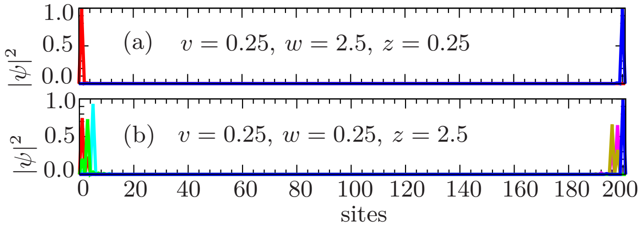

FIG. 20: Probability density of edge states for $H = H_{vw} + H_{z,3}^{\text{B-A}}$: (a) for $v = 0.25$, $w = 2.5$, $z = 0.25$, one pair of edge states, (b) for $v = 0.25$, $w = 0.25$, $z = 2.5$, three pairs of edge states. Figures are drawn for 200 sites.

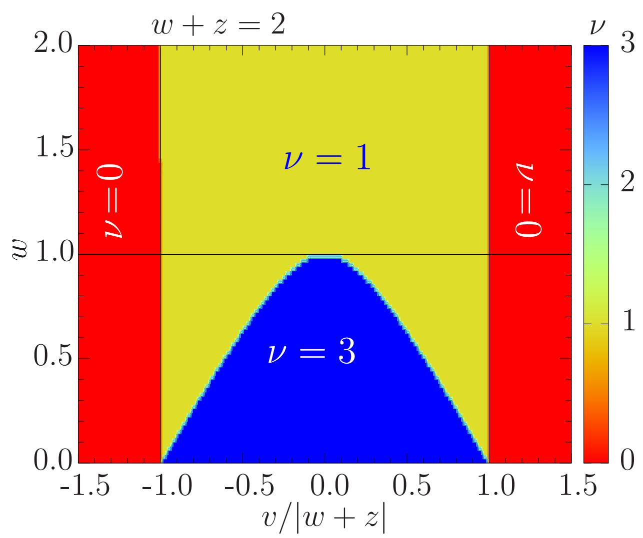

FIG. 21: Topological phase diagram for the Hamiltonian, $H_{z,3}^{\text{B-A}}$. Trivial phase is shown by red ($\nu = 0$) while two distinct topological phases are shown by yellow ($\nu = 1$) and blue ($\nu = 3$). This diagram is drawn for $w+z = 2$. The horizontal line indicates the value $w = 1$ or $w/z = 1$.

the Eqs. $E_\pm(\mathrm{k}) = 0$, and $\frac{dE_\pm(\mathrm{k})}{d\mathrm{k}} = 0$. Combination of those two equations leads to a quadratic equation, $v^2 + w^2 + z^2 + 2\{vwp + wz(2p^2-1) + vzp(4p^2-3)\} = 0$, where $p = \cos^{-1}\left(\frac{-wz\pm\sqrt{w^2z^2-3v^2z(w-3z)}}{6vz}\right)$. Two solutions of this equation along with the constraint, $w+z = 2$, yield the equation of phase transition lines. Those curved lines are symmetric around the straight line $v/(w+z) = 0$.

Trivial phase ($\nu = 0$) appears beyond the two vertical lines drawn at $v/(w+z) = \pm 1$. They separate topological phases with $\nu = 1$ and 3 from the trivial phase. So the system undergoes phase transition around those straight lines. The structure of this phase diagram looks similar to that shown in Fig. 14. However, a closer scrutiny will reveal that the positions of topological phases are different. At the same time parameters plotted along the two axes are also different. Topological phase with $\nu = -2$ is replaced by that of $\nu = 3$ and the trivial phase ($\nu = 0$) and another topological phase with $\nu = 1$ interchange their positions.

According to the formalism for quenching of edge states as discussed before, dynamics of the edge states in the presence of the same nonlinear terms for the topological phases of this model has been studied. The set of coupled nonlinear equation for chain of $L/2$ unit cells and for the Hamiltonian defined in Eq. 18 with OBC is given by

$$\begin{aligned}
i\,\frac{\partial\psi_{2j-1}}{\partial t} &= v(\psi_{2j}-\psi_{2j-1}) + w(\psi_{2j-2}-\psi_{2j-1}) \\
&\quad + z(\psi_{2j-6}-\psi_{2j-1}) - \zeta|\psi_{2j-1}|^2\psi_{2j-1}, \\
\vdots\ &= \qquad\qquad \vdots \\
i\,\frac{\partial\psi_{2j}}{\partial t} &= w(\psi_{2j+1}-\psi_{2j}) + v(\psi_{2j-1}-\psi_{2j}) \\
&\quad + z(\psi_{2j+5}-\psi_{2j}) - \zeta|\psi_{2j}|^2\psi_{2j}.
\end{aligned} \tag{20}$$

Evolution of edge states for the nonlinear system is shown in Fig. 22, by solving the set of Eq. 20, for $L = 20$ when $\zeta = 0.5$. Contour plot for the time evolution of $|\psi_l(t)|$, is drawn for every site which is shown along the horizontal axis. Three contour plots are shown (a) for $v = 2.5$, $w = 0.25$, $z = 0.25$, (b) for $v = 0.25$, $w = 2.5$, $z = 0.25$, (c) for $v = 0.25$, $w = 0.25$, $z = 2.5$, where (a) indicates trivial phase as before while (b) and (c) for the topological phases of $\nu = 1$ and $\nu = 3$, respectively. In this case, initial condition is set by $\psi_l(0) = \delta_{l,m}$, where $m = 1, 3, 5, 16, 18, 20$. As a result, conservation rule is modified by the equation, $\sum_{l=1}^{L} |\psi_l(t)|^2 = 6$ for every case.

Evolution of the system is explored for the time range $0 \le t \le 20$, as shown along the vertical axis. The diagram in (b) clearly indicates that probability amplitudes for $l = 1, 20$, *i. e.*, $|\psi_1(t)|$ and $|\psi_{20}(t)|$ survive with time. So the edge states bound to the topological phase with $\nu = 1$ exhibit their quenching. Obviously, no such quenching is found for any site in the trivial phase as shown in (a). Quenching of amplitudes of wave function for six sites, $|\psi_l(t)|$, when $l = 1, 3, 5, 16, 18, 20$ are found in (c) which correspond to the topological phase with $\nu = 3$. So, quenching will be found for the amplitude with sites $l = 1, 3, 5, L-4, L-2, L$, in case of chain of length L. The number of quenched sites increases with the increase of ν.

F. Topological phases for $H = H_{vw} + H_{z,3}^{\text{A-B}}$

Total Hamiltonian now is

$$\begin{aligned}
H &= H_{vw} + H_{z,3}^{\text{A-B}}, \\
H_{z,3}^{\text{A-B}} &= \sum_{j=1}^{N} z\, c_{\text{A},j}^{\dagger} c_{\text{B},j+3} + \text{h.c.},
\end{aligned} \tag{21}$$

where the hopping term extends over two intermediate primitive cells, as shown in Fig. 23. The components of $\boldsymbol{g}(\mathrm{k})$ in this case are

$$\boldsymbol{g}(\mathrm{k}) \equiv \begin{cases} g_x = v + w\cos(\mathrm{k}) + z\cos(3\mathrm{k}), \\ g_y = w\sin(\mathrm{k}) - z\sin(3\mathrm{k}), \\ g_z = 0. \end{cases}$$

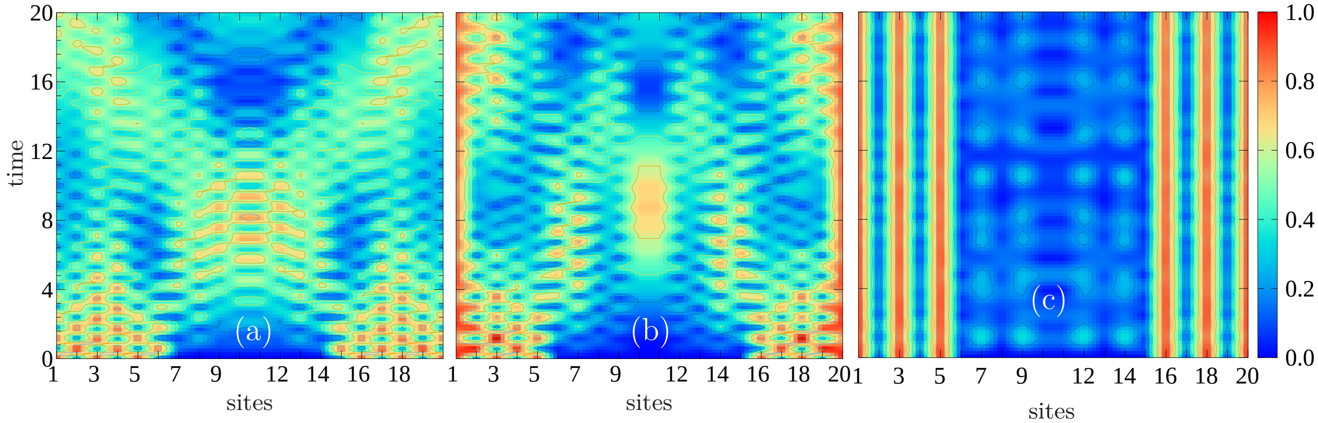

FIG. 22: Quench dynamics for $H = H_{vw} + H_{z,3}^{\text{B-A}}$ when $\zeta = 0.5$, (a) for $v = 2.5$, $w = 0.25$, $z = 0.25$, (b) for $v = 0.25$, $w = 2.5$, $z = 0.25$, (c) for $v = 0.25$, $w = 0.25$, $z = 2.5$. Figures are drawn for lattice of 20 sites.

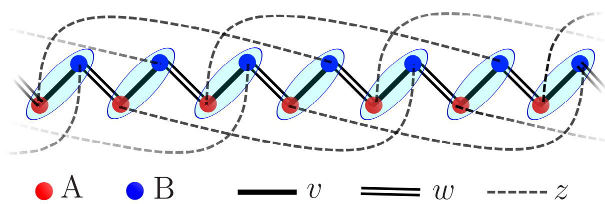

FIG. 23: Extended SSH model describing the hopping in $H = H_{vw} + H_{z,3}^{\text{A-B}}$.

The corresponding dispersion relation is $E_\pm(\text{k}) = \pm\sqrt{v^2 + w^2 + z^2 + 2[vw\cos(\text{k}) + vz\cos(3\text{k}) + wz\cos(4\text{k})]}$. Variation of dispersion relation, $E_+(\text{k})$, with $v/|w+z|$ for $w = 1$, $z = 1/2$ and $w = 1/2$, $z = 1$ are shown in Fig. 24 (a) and (b), respectively for the region $-2 \leq v/|w+z| \leq +2$. Figures for $w > z$ and $w < z$ will be of similar shape as shown in (a) and (b). Dispersions exhibits three broad peaks in the regions away from the point $v/|w+z| = 1$ for both the cases $w/z > 1$ and $w/z < 1$. Again the band gap vanishes at the BZ boundaries, $\text{k} = \pm\pi$, and $\text{k} = 0$ when $v = |w+z|$. As a result, ν is undefined at the point when $v = |w+z|$.

This time, three different nontrivial phases with $\nu = +1, -1$ and -3 appear in the parameter space as given below which are separated by distinct phase transition lines.

$$\nu = \begin{cases} 0, & v > |w+z|, \\ 1, -1 & v < |w+z|, \text{ and } w > z, \\ -3, -1, & v < |w+z|, \text{ and } w < z. \end{cases} \tag{22}$$

Trivial phase exists when $v > |w+z|$. A pair of distinct topological phase with $\nu = \pm 1$ emerges when $v < |w+z|$ and $w > z$. Another pair of nontrivial phase with $\nu = -3$ and -1 appears $v < |w+z|$ when $w < z$. It means the phase with $\nu = -1$ emerges in two different regions when $v < |w+z|$ but for both $w > z$ and $w < z$. The location of this transition point can be determined by satisfying the conditions, $E_\pm(\text{k}) = 0$, and $\frac{dE_\pm(\text{k})}{d\text{k}} = 0$. So, this model is capable to host a new topological phase with $\nu = -3$.

The parametric plot of winding by the tip of the vector, $\boldsymbol{g}(\text{k})$ in the g_x-g_y plane are shown in Fig. 25. Four figures are drawn for (a) $v = 1.0$, $w = 0.5$, $z = 0.4$, (b) $v = 0.3$, $w = 0.6$, $z = 0.5$, (c) $v = 0.2$, $w = 0.3$, $z = 0.6$, and (d) $v = 0.5$, $w = 0.4$, $z = 0.3$. Curves shown in (a) and (d) traverse along the counter clockwise direction, while those in (b) and (c) traverse along the clockwise direction. As a result the winding number for (d) is positive, but that for (b) and (c) is negative. Those figures can be regarded as prototype contours for the four different regions. For example, the phase is trivial ($\nu = 0$), for any values of v, w and z as long as $v > |w+z|$. On the other hand, four different regions are identified when $v < |w+z|$, where distinct topological phases appear. A pair of phases appear for $w > z$ and another pair for $w < z$. Nonzero band gap exists for all the cases.

Variation of bulk-edge state energies with respect to $v/|w+z|$ is shown in Fig. 26 for the regime $-2 \leq (v/|w+z|) \leq 2$. Zero energy edge states emerges as long as $-1 \leq (v/|w+z|) \leq 1$, which is consistent to the previous observation. So, no edge state is there in this system when $v > |w+z|$. However, three pairs of zero energy edge states appear in a region around the point $v/|w+z| = 0$ when $v < |w+z|$ and $w < z$ which is shown in Fig. 26 (b). This particular region is surrounded by another topological phase with $\nu = -1$ as long as $-1 \leq (v/|w+z|) \leq 1$. The figures are drawn for lattice of sites 200, and the results conform to the bulk-edge correspondence rule in the topological phases.

In order to confirm the existence of zero energy edge states, probability density of those states are drawn in Fig. 27 for the lattice of 200 sites. Two figures are drawn for two distinct topological phases. In the upper panel (a), probability densities of two distinct edge states with $E = 0$ are shown when $v = 0.25$, $w = 2.5$, $z = 0.25$. Those values are selected for satisfying the conditions, $v < |w+z|$ and $w > z$. Probability density of one edge state exhibits sharp peak at site $m = 1$ and another one at site $m = 200$. This corresponds to the topological phase with $\nu = 1$. On the other hand, for $v < |w+z|$ and $w < z$, probability density of six distinct zero energy edge states

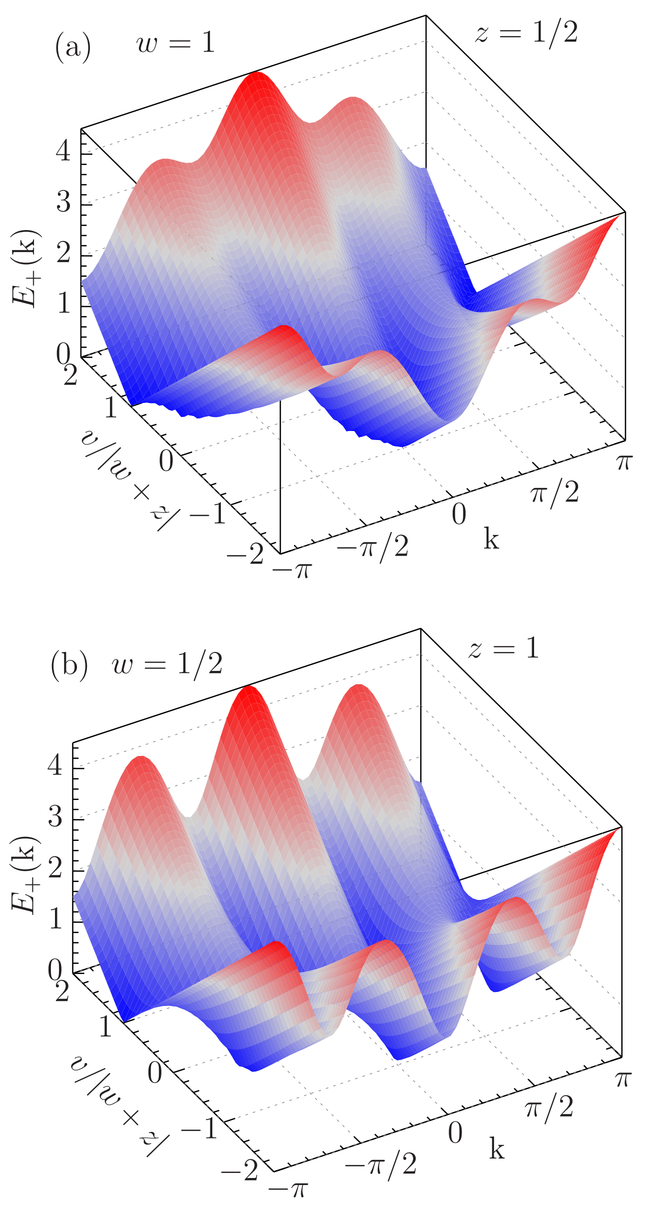

FIG. 24: Dispersion relation for $H = H_{vw} + H_{z,3}^{\text{A-B}}$ when $w/z > 1$, (a) and $w/z < 1$, (b).

are shown in the lower panel (b) when $v = 0.25$, $w = 0.25$, $z = 2.5$. Probability density of six orthonormal edge states exhibit sharp peak at sites $m = 2, 4, 6, 195, 197$ and 199. This result is in accordance to the topological phase of $\nu = -3$. Localization of zero energy states are found on B sublattice near left edge and A sublattice near right edge.

A rigorous phase diagram for this model is shown in Fig 28, where contour plot for ν is drawn in the w-$v/|w+z|$ space. Variation of the parameters is made by maintaining the constraint $w + z = 2$. The existence of three different topological phases, $\nu = \pm 1$ and -3 along with the trivial phase, $\nu = 0$ is shown in four different colors. The horizontal line is drawn at $w/z = 1$, which separates the topological phase with $\nu = 1$ from that with $\nu = -3$. Three topolgical phases meet at the point, $v/(w+z) = 0$, $w = 1$. All the topological phases remain within the region bounded by the vertical lines drawn at

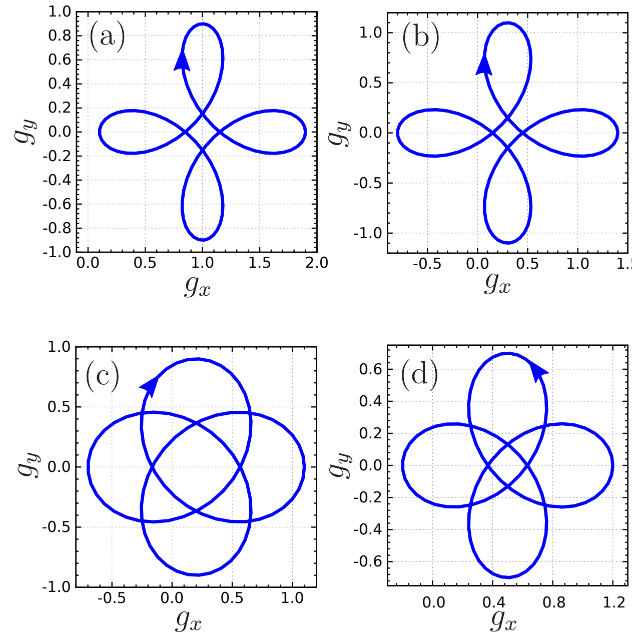

FIG. 25: Parametric winding diagrams in the g_x-g_y plane for the Hamiltonian, $H = H_{vw} + H_{z,3}^{\text{A-B}}$. Four figures are drawn for (a) $v = 1.0$, $w = 0.5$, $z = 0.4$, (b) $v = 0.3$, $w = 0.6$, $z = 0.5$, (c) $v = 0.2$, $w = 0.3$, $z = 0.6$, and (d) $v = 0.5$, $w = 0.4$, $z = 0.3$.

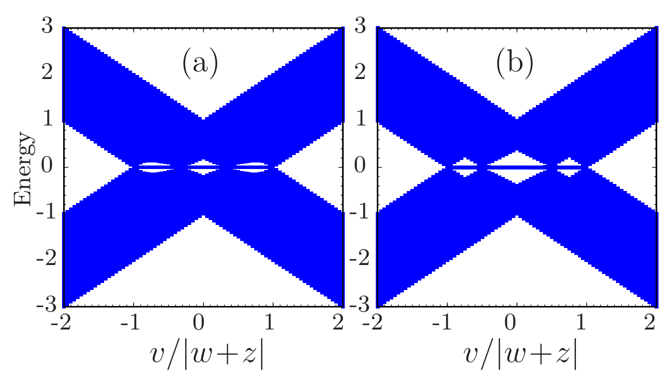

FIG. 26: Edge states for $H = H_{vw} + H_{z,3}^{\text{A-B}}$ when $w/z > 1$, (a) for $w = 0.6$, $z = 0.4$, and $w/z < 1$, (b) for $w = 0.3$, $z = 0.7$.

$v/(w+z) = \pm 1$. So the trivial phase lies beyond the region $-1 \leq v/(w+z) \leq +1$ for any value of w. The curved boundary lines separating the nontrivial phases can be obtained from the solutions of the Eqs. $E_\pm(\mathrm{k}) = 0$, and $\frac{dE_\pm(\mathrm{k})}{d\mathrm{k}} = 0$. Those equations yield a cubic equation, whose solutions along with the constraint, $w + z = 2$, provides the equation of transition lines.

According to the formalism for quenching of edge states as discussed before, dynamics of the edge states in the presence of nonlinear terms for the topological phases of this model will be discussed. The set of coupled nonlinear equation for chain of L lattice sites and for the

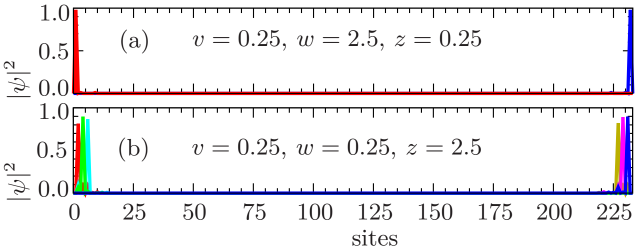

FIG. 27: Probability density of edge states for $H = H_{vw} + H_{z,3}^{\text{A-B}}$: (a) for $v = 0.25$, $w = 2.5$, $z = 0.25$, one pair of edge states, (b) for $v = 0.25$, $w = 0.25$, $z = 2.5$, three pairs of edge states. Figures are drawn for 232 sites.

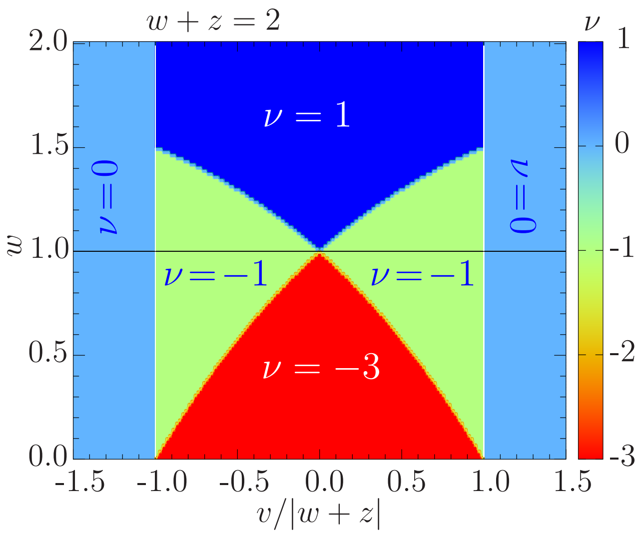

FIG. 28: Topological phase diagram for the Hamiltonian $H = H_{vw} + H_{z,3}^{\text{A-B}}$. Three distinct topological phases are shown by blue ($\nu = 1$), green ($\nu = -1$) and red ($\nu = -3$). The remaining portion is trivial ($\nu = 0$). This diagram is drawn for $w + z = 2$. The horizontal line indicates the value $w = 1$ or $w/z = 1$.

Hamiltonian defined in Eq. 21 with OBC is given by

$$
\begin{aligned}
i\,\frac{\partial \psi_{2j-1}}{\partial t} &= v(\psi_{2j} - \psi_{2j-1}) + w(\psi_{2j-2} - \psi_{2j-1}) \\
&\quad + z(\psi_{2j+6} - \psi_{2j-1}) - \zeta|\psi_{2j-1}|^2\psi_{2j-1}, \\
\vdots \quad &= \quad \vdots \\
i\,\frac{\partial \psi_{2j}}{\partial t} &= w(\psi_{2j+1} - \psi_{2j}) + v(\psi_{2j-1} - \psi_{2j}) \\
&\quad + z(\psi_{2j-7} - \psi_{2j}) - \zeta|\psi_{2j}|^2\psi_{2j}.
\end{aligned}
\tag{23}
$$

Evolution of edge states for the nonlinear system is shown in Fig. 29, by solving the set of Eq. 23, for $L = 20$ when $\zeta = 0.5$. Contour plot for the time evolution of $|\psi_l(t)|$, is drawn for every site which is shown along the horizontal axis. Three contour plots are shown (a) for $v = 2.5$, $w = 0.25$, $z = 0.25$, (b) for $v = 0.25$, $w = 2.5$, $z = 0.25$, (c) for $v = 0.25$, $w = 0.25$, $z = 2.5$, where (a) indicates trivial phase as before while (b) and (c) for the topological phases of $\nu = -1$ and $\nu = -3$, respectively. In this case, initial condition is set by $\psi_l(0) = \delta_{l,m}$, where $m = 2, 4, 6, 16, 18, 20$. As a result, conservation rule is modified by the equation, $\sum_{l=1}^{L} |\psi_l(t)|^2 = 6$, for every case.

Evolution of the system is explored for the time range $0 \le t \le 20$, as shown along the vertical axis. The diagram in (b) clearly indicates that probability amplitudes for $l = 1, 20$, *i. e.*, $|\psi_1(t)|$ and $|\psi_{20}(t)|$ survive with time. So, the edge states bound to the topological phase with $\nu = 1$ exhibit their quenching. Obviously, no such quenching is found for any site in the trivial phase as shown in (a). Quenching of amplitudes of wave function for six sites, $|\psi_l(t)|$, when $l = 2, 4, 6, 15, 17, 19$ is found in (c) which correspond to the topological phase with $\nu = -3$. Therefore, quenching will be found in general for the amplitudes on sites $l = 2, 4, 6, L-5, L-3, L-1$, if a chain of length L is considered. Again, the quenched sites for A and B sublattices interchange the edges with respect to the last case. So the phase with higher values of ν can be studied where the quenching of absolute value of the probability amplitude for higher number of sites close to the ends of the lattice is observed.

Summarizing the results of above findings it is concluded that the method proposed in this work by constructing series of Hamiltonians, $H = H_{vw} + H_{z,m}^{\text{B-A}}$, and $H = H_{vw} + H_{z,m}^{\text{A-B}}$, with $m = 1, 2, 3, \cdots$, topological phases with $\nu = \pm1, \pm2, \pm3, \cdots$, can be realized. Only one further neighbour hopping term of strength z is introduced within the standard SSH model, whose extent is determined by the integer m. In this formulation, m denotes the extent of further neighbor hopping which passes over $(m - 1)$ intermediate cells. With the increase of m, topological phases of higher values of ν will be realized. Hamiltonians of the type $H = H_{vw} + H_{z,m}^{\text{B-A}}$, yield phases of positive winding number only, while that of type $H = H_{vw} + H_{z,m}^{\text{A-B}}$, yield those of negative winding numbers along with $\nu = 0$ and $\nu = +1$. A list of Hamiltonians along with the winding numbers of accompanying phases are given in Tab. 1.

m	$H = H_{vw} + H_{z,m}^{\text{B-A}}$	$H = H_{vw} + H_{z,m}^{\text{A-B}}$
1	$\nu = 0, 1$	$\nu = -1, 0, 1$
2	$\nu = 0, 1, 2$	$\nu = -2, 0, 1$
3	$\nu = 0, 1, 3$	$\nu = -3 - 1, 0, 1$
4	$\nu = 0, 1, 2, 4$	$\nu = -4, -2, 0, 1$
5	$\nu = 0, 1, 3, 5$	$\nu = -5, -3, -1, 0, 1$
$\vdots$	$\vdots$	$\vdots$
$2p$	$\nu = 0, 1, 2, \cdots, 2p$	$\nu = -2p, -2p+2, \cdots, -2, 0, 1$
$2p+1$	$\nu = 0, 1, 3, \cdots, 2p+1$	$\nu = -2p-1, -2p+1, \cdots, -1, 0, 1$

TABLE I: Distribution of winding numbers with the value of m for the Hamiltonians $H = H_{vw} + H_{z,m}^{\text{B-A}}$ and $H = H_{vw} + H_{z,m}^{\text{A-B}}$. Here p is integer.

From this table, it is evident that, the topological phase with $\nu = 1$ and the trivial phase are present in every case. Apart from these common phases, an ‘odd-even’

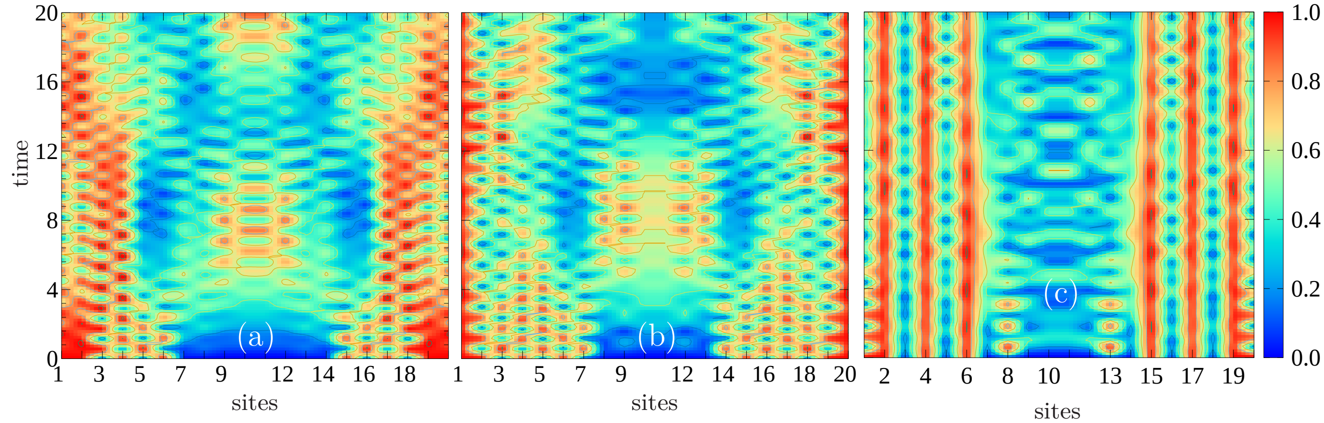

FIG. 29: Quench dynamics for $H = H_{vw} + H_{z,3}^{\text{A-B}}$ when $\zeta = 0.5$, (a) for $v = 2.5$, $w = 0.25$, $z = 0.25$, (b) for $v = 0.25$, $w = 2.5$, $z = 0.25$, (c) for $v = 0.25$, $w = 0.25$, $z = 2.5$. Figures are drawn for lattice of 20 sites.

effect for the values of ν is found with respect to m. In addition to $\nu = 0, 1$ only even (odd) values of ν appear when m is even (odd). This is true for both 'B-A' and 'A-B' types of Hamiltonians. Also, number of nontrivial phases increases with the value of m for both types of Hamiltonians. The result is generalized in the last two rows of the table, which refer to even, $(m = 2p)$ and odd $(m = 2p + 1)$ values of m, where p is an integer. More precisely, the number of nontrivial phase is equal to the value of $(p + 1)$ and $(p + 2)$, respectively, for 'B-A' and 'A-B' types of Hamiltonians when $m = (2p + 1)$ (odd). For even $m = 2p$, both 'B-A' and 'A-B' types yield $(p+1)$ number of topological phase.

Another interesting finding is that, in order to realize the topological phase of the largest possible values of winding numbers from a specific Hamiltonian, value of z is to be made larger than the individual values of v and w. More elaborately, it is known that maximum value of ν for the topological phase host by $H = H_{vw} + H_{z,m}^{\text{B-A}}$ is $+m$, while that host by $H = H_{vw} + H_{z,m}^{\text{A-B}}$ is $-m$. However, this particular phase cannot be generated from the relevant Hamiltonian by substituting any value of v/z and w/z. By examining the phase diagrams as depicted in the Figs. 7, 14, 21, and 28, it can be concluded that the phase of the maximum value of ν can be achieved easily by choosing the values of the parameters in such a way that they must satisfy the relations: $v/z \to 0$, and $w/z \to 0$. These limiting values indicate that phase with the maximum value of ν emerges when both the inter and intracell hopping strength are much weaker than that of the further neighbour cells.

Figs. (b) in 6, 13, 20 and 27 indicate that localization of symmetry-protected zero energy states are found on A and B sublattices in a different way for phases with +ve and −ve values of ν. For $\nu > 0$, localization are found on A sublattice for left edge and on B sublattice for right edge. But the localization occurs in the opposite fashion when $\nu < 0$.

IV. TOPOLOGICAL PHASES IN TERMS OF CHERN NUMBERS

In this case, further neighbour hoppings are allowed within the same types of sublattice, means between A-A and B-B types of sites. In addition, further neighbour hoppings are limited between the NN cells. The simplest model which exhibits topological phases with any values of Chern numbers is defined by the Hamiltonian,

$$\begin{aligned} H &= H_{vw} + H_t, \\ H_t &= \sum_{j=1}^{N} \Big(t_a\, c_{\text{A},j}^\dagger c_{\text{A},j+1} + t_b\, c_{\text{B},j}^\dagger c_{\text{B},j+1} \Big) + \text{h.c.}, \end{aligned} \tag{24}$$

where t_a and t_b denote respectively the hopping param-

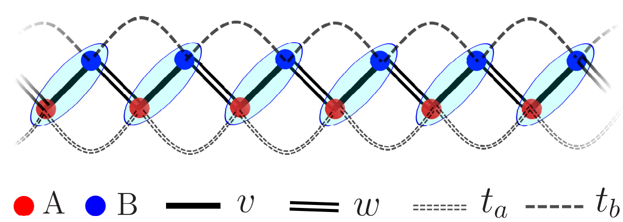

FIG. 30: Extended SSH model describing the hopping for the Hamiltonian in Eq. 24.

eters between A-A and B-B types of sites belonging to the NN cells. The model is described in the Fig. 30. Assuming PBC, the Hamiltonian in the k-space becomes $H(\text{k}) = g_I(\text{k}) I + \boldsymbol{g}(\text{k}) \cdot \boldsymbol{\sigma}$, where I is the 2×2 identity matrix, $g_I(\text{k}) = (t_a + t_b)\cos(\text{k})$, and

$$\boldsymbol{g}(\text{k}) \equiv \begin{cases} g_x = v + w\cos(\text{k}), \\ g_y = w\sin(\text{k}), \\ g_z = (t_a - t_b)\cos(\text{k}). \end{cases}$$

Since $\boldsymbol{g}(\text{k})$ is a three-component vector, chiral symmetry is not preserved for this model. In addition particle-hole and inversion symmetries are not preserved. The

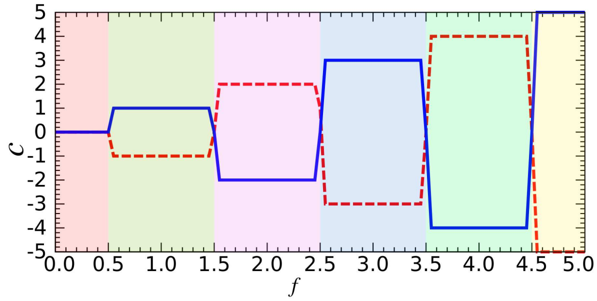

FIG. 31: Variation of $\mathcal{C}$ with f for the Hamiltonian defined in Eq. 24 with the parameters in Eq. 27 is shown. Phases with higher values of $\mathcal{C}$ will appear with the increase of f. Solid blue line for $\phi = (n+\frac{1}{2})\pi$, and dashed red line for $\phi = (n-\frac{1}{2})\pi$.

standard forms of those symmetries for 1D system now satisfy

$$\begin{cases} \mathcal{P}H(\mathrm{k})\mathcal{P}^{-1} \neq -H(-\mathrm{k}), \\ \sigma_x H(\mathrm{k})\sigma_x \neq H(-\mathrm{k}), \\ \sigma_z H(\mathrm{k})\sigma_z \neq -H(\mathrm{k}). \end{cases}$$

However, those symmetries in the k-θ space can be restored by choosing the hopping terms accordingly. No topological phase in terms of nonzero winding number is present in this case. However, this model is capable to behave like an effective 2D model in the virtual momentum space if the amplitude of hopping parameters are modulated cyclically in terms of two additional angular parameters θ and ϕ. Li *et al* introduced this model and reported the emergence of topological phases characterized by the Chern numbers of Haldane like two-band 2D system[32]. Parametrization behind the realization of this phase is

$$\begin{cases} v = t[1+\delta\cos(\theta)], \\ w = t[1-\delta\cos(\theta)], \\ t_a = h\,\cos(\theta+\phi), \\ t_b = h\,\cos(\theta-\phi). \end{cases} \tag{25}$$

Investigation on this model has been carried out under periodic drive in order to find Floquet topological phase[30].

The Hamiltonian with this parametrization preserve the inversion symmetry in terms of two variables k and θ, since

$$\sigma_x H(\mathrm{k},\theta)\sigma_x = H(-\mathrm{k},-\theta),$$

for any values of ϕ, as long as $\theta \neq 0$. In addition, Hamiltonian preserves the mirror symmetry with respect to θ, when $\phi = 0, \pm m\pi$, where m is integer. Let $\mathcal{M}_\theta$ be the operator for mirror symmetry and it acts as, $\mathcal{M}_\theta g(\theta) = g(-\theta)$, where $g(\theta)$ is an arbitrary function of θ. Hamiltonian obeys the relation,

$$\mathcal{M}_\theta H(\mathrm{k},\theta)\mathcal{M}_\theta^{-1} = H(\mathrm{k},\theta),$$

only for $\phi = 0, \pm m\pi$. Anyway, this symmetry is not relevant to the topological properties in this case. However, Hamiltonian preserves the mirror symmetry with respect to both θ, and ϕ. It means, if $\mathcal{M}_{\theta,\phi}$ be the operator of that symmetry, Hamiltonian holds the relation:

$$\mathcal{M}_{\theta,\phi} H(\mathrm{k},\theta)\mathcal{M}_{\theta,\phi}^{-1} = H(\mathrm{k},\theta).$$

It occurs due to the fact that hopping parameters, v, w, t_a and t_b do not change sign upon simultaneous sign reversal of angular variables θ and ϕ.

Interestingly, topological phase of 2D system is realized in this 1D model when θ is allowed to vary from $-\pi$ to π, for a specific value of another angular variable ϕ. For example, $\mathcal{C} = \pm 1$ is realized when $0 < \phi < \pi$, while $\mathcal{C} = \mp 1$ when $-\pi < \phi < 0$. Mirror symmetry with respect to $\mathcal{M}_\theta$ is broken in this entire regime, but that with respect to $\mathcal{M}_{\theta,\phi}$ is preserved. Band gap vanishes for $\phi = 0$, as well as band inversion occurs around this point. Hence these two distinct topological phases are realized in this model. No other phase is realized if the further neighbour hopping extends beyond the NN primitive cells for the parametrization defined in Eq. 25. However, band inversion is found to take place if further neighbor hopping between NN cells is replaced by NNN cells and this phenomenon occurs recursively if the further neighbor hopping terms extend beyond NNN cells successively in addition.

Chern number can be defined in this virtual reciprocal space as

$$\mathcal{C} = \frac{1}{2\pi}\iint\limits_{\mathrm{BZ}} d\mathrm{k}d\theta\,(\partial_\theta A_\mathrm{k} - \partial_\mathrm{k} A_\theta), \tag{26}$$

where the Berry phase, $A_\nu = i\langle \mathrm{k}\theta|\partial_\nu|\mathrm{k}\theta\rangle$, with $\nu = \mathrm{k}, \theta$ and $|\mathrm{k}\theta\rangle$ is the Bloch state. Integration is performed over the BZ in the 2D reciprocal space. The reciprocal space is called virtual in a sense that no parameter in the real space can be connected to the angular variable θ, as on contrary the wave number k corresponds to the reciprocal of the lattice parameter for the real space. In order to find the Chern number the integral in Eq 26 is numerically evaluated[37].

In this study, new topological phases other than $\mathcal{C} = \pm 1$ and ∓ 1 have been obtained in a very simple way in which the angular variable θ is replaced by $(f\theta)$ where f may assume any values. Another cyclic parameter ϕ also depends on f as shown below. Higher values of f lead to phases with higher values of $\mathcal{C}$. In other words for the realization of phases with $\mathcal{C} = \pm n$ and $\mp n$, with $n = 1, 2, 3, \cdots$, sequentially, the following parametrization is implemented,

$$\begin{cases} v = t[1+\delta\cos(f\theta)], \\ w = t[1-\delta\cos(f\theta)], \\ t_a = h\,\cos(f\theta+\phi), \\ t_b = h\,\cos(f\theta-\phi), \end{cases} \tag{27}$$

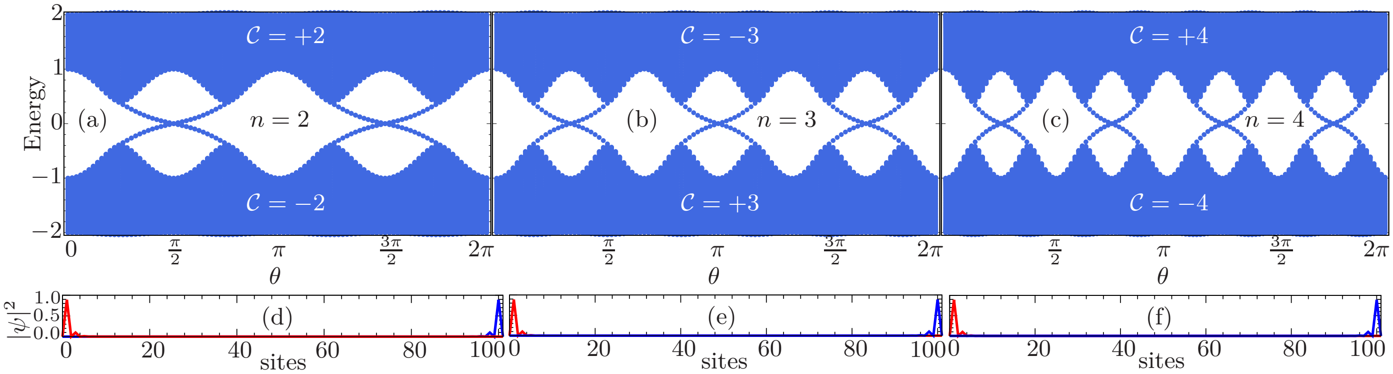

FIG. 32: Variation of energy with θ for the Hamiltonian defined in Eq. 24 and the parametrization defined in Eq. 27 are drawn in the upper panel. Figures are drawn for $t = 1$, $\delta = 0.5$, $h = 0.2$, $\phi = (n + \frac{1}{2})\pi$ and $n = 2$ in (a), $n = 3$ in (b), $n = 4$ in (c). Figures are drawn for lattice of 100 sites. Probability density of the corresponding edge states are shown in the lower panel. $\theta = \pi/2$ when $n = 2$ in (d), $\theta = (\pi - 1)/2$ when $n = 3$ in (e), and $\theta = \pi/4$ when $n = 4$ in (f).

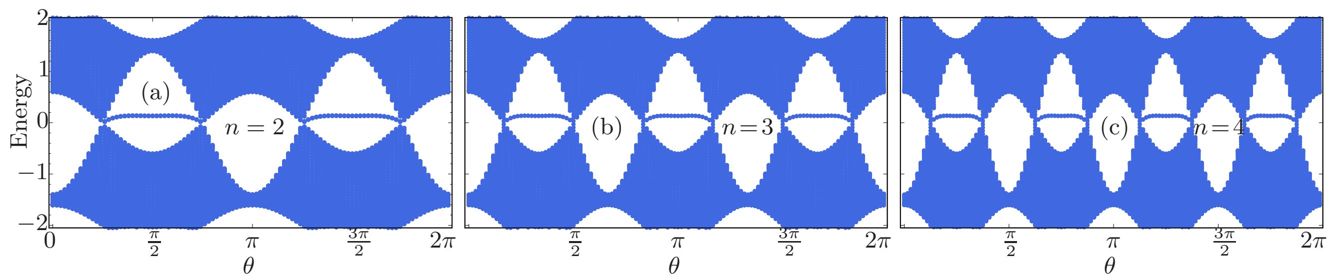

FIG. 33: Variation of energy with θ for the Hamiltonian defined in Eq. 24 and the parametrization defined in Eq. 27 are drawn when $\phi = 0$. Figures are drawn for $t = 1$, $\delta = 0.5$, $h = 0.2$, and $n = 2$ in (a), $n = 3$ in (b), $n = 4$ in (c). Figures are drawn for lattice of 100 sites.

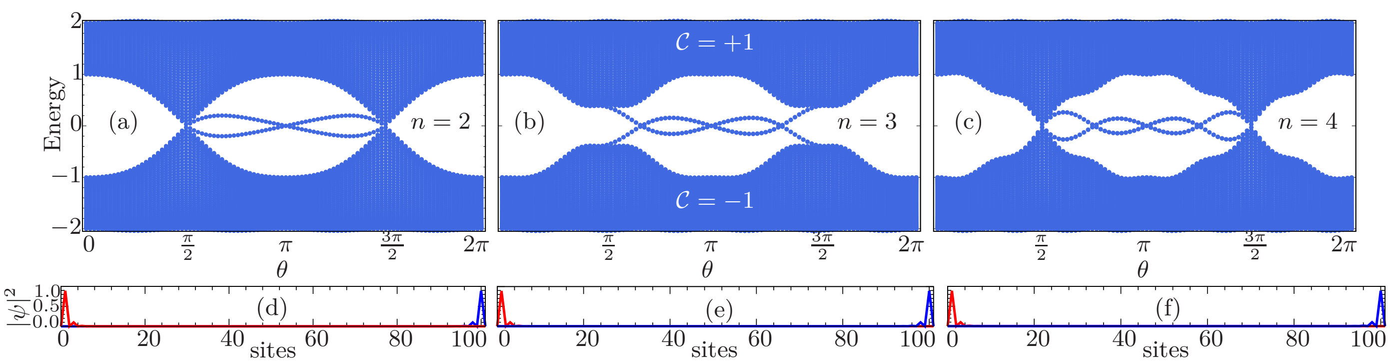

FIG. 34: Variation of energy with θ for the Hamiltonian defined in Eq. 24 and the parametrization defined in Eq. 28 are drawn in the upper panel. Figures are drawn for $t = 1$, $\delta = 0.5$, $h = 0.2$, $\phi = \pi/2$ and $n = 2$ in (a), $n = 3$ in (b), $n = 4$ in (c). Figures are drawn for lattice of 100 sites. Probability density of the corresponding edge states when $\theta = \pi$ are shown in the lower panel for $n = 2$ in (d), $n = 3$ in (e), and $n = 4$ in (f).

where $\phi = (f \pm \frac{1}{2})\pi$. The mirror symmetry with respect to the operator, $\mathcal{M}_\theta$ is preserved only when $f = \pm\frac{1}{2}, \pm\frac{3}{2}, \pm\frac{5}{2}, \cdots$. Because at those points all the hopping parameters, v, w, t_a and t_b do not change sign upon the sign reversal of angular variable θ. So, the Hamiltonian remains invariant under the transformation. In contrast, the particle-hole symmetry is preserved in the k-θ space only when f is integer, since the relation,

$$\mathcal{P}H(\mathrm{k},\theta)\mathcal{P}^{-1} = -H(-\mathrm{k},-\theta),$$

is satisfied at those points. But the chiral symmetry is not preserved anymore.

The system is found to host nontrivial phases with

$$\mathcal{C} = \begin{cases} \pm n, & (n-\frac{1}{2}) < f < (n+\frac{1}{2}), \text{ when } n = 1,3,5,\cdots, \\ \mp n, & (n-\frac{1}{2}) < f < (n+\frac{1}{2}), \text{ when } n = 2,4,6,\cdots, \end{cases}$$

when $\phi = (f + \frac{1}{2})\pi$. On the other hand, it yields

$$\mathcal{C} = \begin{cases} \mp n, & (n-\frac{1}{2}) < f < (n+\frac{1}{2}), \text{ when } n = 1,3,5,\cdots, \\ \pm n, & (n-\frac{1}{2}) < f < (n+\frac{1}{2}), \text{ when } n = 2,4,6,\cdots, \end{cases}$$

when $\phi = (f - \frac{1}{2})\pi$. $\mathcal{C}$ is undefined when $f = \frac{1}{2}, \frac{3}{2}, \frac{5}{2}, \cdots$, as band gap closes at those points when $\phi = (f \pm \frac{1}{2})\pi$. At these points the system preserves the mirror symmetry, $\mathcal{M}_\theta$. Which means topological phase emerges when this mirror symmetry is broken.

Appearance of topological phases with increasing Chern numbers with the increase of f is shown in Fig. 31. Topological phases $\mathcal{C} = \pm1, \pm2, \pm3, \pm4$ and ±5 are shown here. New phases with higher values of $\mathcal{C}$s may appear with the increase of f. Chern number is undefined at the intermediate points when $f = \frac{1}{2}, \frac{3}{2}, \frac{5}{2}, \cdots$. This phase diagram is independent of the value of t, δ and h.

In order to visualize the edge states, variation of energy with θ is shown in the upper panel of Fig. 32. A chain of 100 sites is considered. Figures are drawn for $t = 1$, $\delta = 0.5$, $h = 0.2$, $\phi = (n + \frac{1}{2})\pi$ and $n = 2$ in (a), $n = 3$ in (b), $n = 4$ in (c). n pairs of edge state lines are found for each case when $\mathcal{C} = \pm n$. Those results are consistent with the 'bulk-boundary correspondence' rule which states that: chern number is equal to the number of pair of edge states in the gap for the two-band model[34–36]. Probability density of a specific pair edge states for a definite value of θ is shown in the respective lower panels. For example, $\theta = \pi/2$ when $n = 2$ in (d), $\theta = (\pi - 1)/2$ when $n = 3$ in (e), and $\theta = \pi/4$ when $n = 4$ in (f). Variation of energy with θ is shown Fig. 33 when $\phi = 0$ for $t = 1$, $\delta = 0.5$, $h = 0.2$. Value of $\mathcal{C}$ is undefined as there is no band gap when $\phi = 0$. Particle-hole symmetry is not preserved in this case.

For another type of parametrization, where

$$\begin{cases} v = t[1 + \delta\cos(\theta)], \\ w = t[1 - \delta\cos(\theta)], \\ t_a = h\cos(n\theta + \phi), \\ t_b = h\cos(n\theta - \phi), \end{cases} \tag{28}$$

a single topological phase with $\mathcal{C} = \pm1$ always appear when $n = 1,3,5,\cdots$. $\mathcal{C}$ is undefined when $n = 2,4,6,\cdots$ as band gap closes for the even n. Interestingly edge states appear for the trivial phases instead. Not only that, multiple crossing of the edge state energy lines are found for both trivial and topological phases where the number of crossing points are exactly equal to the value of n. Bulk-edge energy dispersion and probability density of the edge states for this parametrization are shown in Fig. 34. In the upper panel bulk-edge energy variation with θ is shown for $n = 2$ in (a), $n = 3$ in (b), and $n = 4$ in (c). Values of the fixed parameters are $t = 1$, $\delta = 0.5$, $h = 0.2$, and $\phi = \pi/2$. Lower panel shows the probability densities of edge states in (d), (e) and (f) for the respective cases. Figures are drawn for lattice of 100 sites.

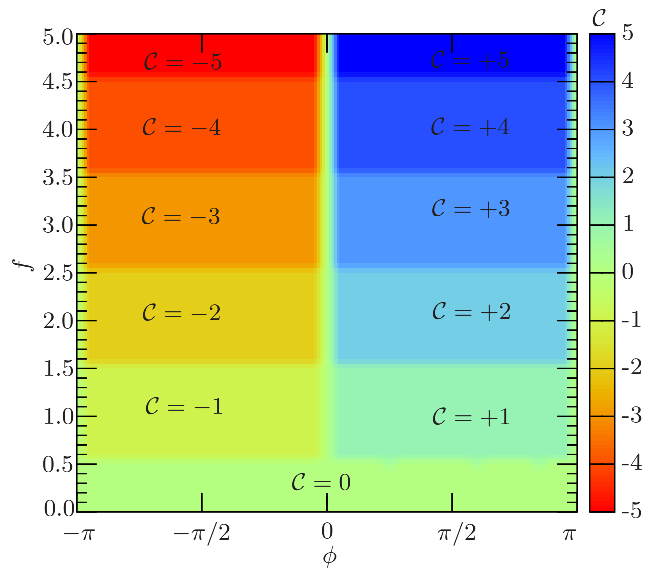

FIG. 35: Variation of $\mathcal{C}$ in the f-ϕ phase space for the Hamiltonian defined in Eq. 24 with the parameters in Eq. 27 is shown but when $-\pi < \phi < \pi$.

Variation of $\mathcal{C}$ in the f-ϕ phase space for the Hamiltonian defined in Eq. 24 with the parameters in Eq. 27 is shown in Fig. 35 but when $-\pi < \phi < \pi$. In this particular case ϕ does not depend on the parameter f. Phases with different values of $\mathcal{C}$ will appear with the increase of f along the vertical axis. However, in this case phases with different $\mathcal{C}$s are not separated by band gap closing. The Hamiltonian remains invariant under the transformation of $\mathcal{M}_{\theta,\phi}$ for any value of f. In contast, symmetry with respect to $\mathcal{M}_\theta$, is preserved only when $f = 0, \pm\pi$. The states shown in Fig. 35 are no more topological in nature since they are not separated by vanishing band gap. In contrast, phases across the line $\phi = 0$ are separated by zero band gap.

V. DISCUSSION

In this investigation, emergence of two different series of topological phases with $\nu = \pm1, \pm2, \pm3, \cdots$, and $\mathcal{C} = \pm1, \pm2, \pm3, \cdots$, has been successfully demonstrated using the 1D eSSH models. The manuscript is composed of two main parts, say Sec IV and III, where the major results are presented. In the first case, a single further neighbor hopping term beyond NN is found enough for the realization of the series of new phase where particle-hole and inversion symmetries are preserved. Those phases can be realized by adding multiple further neighbor terms as well. In the second case, a single pair of NNN hopping terms is found sufficient for the realization of the series of new phases where the standard forms of particle-hole and inversion symmetries for 1D are not preserved.

Four different eSSH models in the first case have been considered in which extend of further neighbor hopping is limited by $m = 2, 3$, and their properties have been studied rigorously. Topological properties have been characterized in terms of winding number, edge states and quench dynamics in the presence of an additional nonlinear term. Finally, the results are generalized for $m > 2$, where phases with higher values of ν appear. Comprehensive phase diagrams are drawn, where the equations of phase transition lines are obtained. It is also expected that a pair of further neighbor staggered hopping terms with varying extent can yield series of topological phases with different ν, however, this case is not addressed here.

It is known that topological interface states emerge when two lattices with different topological phases are joined. Nowadays, study on these interface states in phononic crystals have been initiated[9]. So, the results obtained for these tight-binding models will become helpful for constructing the phononic model in order to realize the topological phase of any desired winding number, as well as to study the properties of interface states. In addition, the most simple route for the demonstration of topological phase of higher winding numbers using systems of ultracold atoms in optical lattice can be obtained by mimicking the structure of these tight-binding models.

In the second case, emergence of topological phase with any value of $\mathcal{C}$ is discussed when the NN and NNN hopping terms in the two-band eSSH model are expressed in terms of two angular variables, θ and ϕ. Particle-hole and inversion symmetries are preserved in the k-θ space. Three different types of parametrization are employed when θ and ϕ depend on another parameter f in three different ways. A specific parametrization gives rise to a nontrivial phase of any value of $\mathcal{C}$ which is controlled by the parameter f. Phase transition points are marked on the phase diagram where the band gap vanishes. Experimental realization of these phases using systems of ultracold atoms in optical lattice is possible, as discussed here[32].

The system hosts topological phases with $\mathcal{C} = \pm 1, \mp 1$, for another parameterization, but with peculiar types of edge states. Here, multiple crossing between the edge states lines is found within the band gap. This particular phenomenon of multiply-crossed edge states as shown in Fig 34 is not reported before. In addition, fake topological phases with series of different $\mathcal{C}$s appear in the third kind of parametrization. They are spurious because of the fact that the band gap does not vanish at the transition points in this case. All the results obtained in this study are insensitive to the external magnetic field. This is because of the fact that there is no spin dependent term in the Hamiltonians. Magnetic field will be registered here as an additional constant in the diagonal element of (2×2) $H(\mathrm{k})$ matrix in every case. As a result, symmetry of this matrix does not change in the presence of magnetic field and all the results remain valid.

VI. ACKNOWLEDGMENTS

RKM acknowledges the DST/INSPIRE Fellowship/2019/IF190085. Authors acknowledge the fruitful discussion with Oindrila Deb.

* Electronic address: rkmalakar75@gmail.com
† Electronic address: asimk.ghosh@jadavpuruniversity.in

[1] W. Su, J. Schrieffer and A. J. Heeger, Phys. Rev. Lett. **42**, 1698 (1979).
[2] Heeger A. J., Kivelson S., Schrieffer J. R. and Su W. -P., Rev. Mod. Phys. **60**, 781 (1988).
[3] A. Y. Kitaev, Phys. -Usp. **44**, 131, (2001)
[4] Y. -X. Chen and S.-W. Li, Phys. Rev. A **81**, 032120 (2010).
[5] J. D. Sau, R. M. Lutchyn, S. Tewari, S. Das Sarma, Phys. Rev. Lett. **104**, 040502 (2010).
[6] M. Atala, M. Aidelsburger, J. T. Barreiro, D. Abanin, T. Kitagawa, E. Demler, and I. Bloch, Nature Physics **9**, 795 (2013).
[7] T. Kitagawa, M. A. Broome, A. Fedrizzi, M. S. Rud- ner, E. Berg, I. Kassal, A. Aspuru-Guzik, E. Demler, and A. G. White, Nature communications **3**, 1 (2012).
[8] Rechtsman M C, Zeuner J M, Plotnik Y, Lumer Y, Podolsky D, Dreisow F, Nolte S, Segev M and Szameit A, Nature **496**, 196 (2013)
[9] Xin Li, Yan Meng, Xiaoxiao Wu, Sheng Yan, Yingzhou Huang, Shuxia Wang, and Weijia Wen, Appl. Phys. Lett. **113**, 203501 (2018)
[10] Z Fu, N Fu, H Zhang, Z Wang, D Zhao and S Ke, Appl. Sci. **10**, 3425 (2020)
[11] M Maffei, A Dauphin, F Cardano, M Lewenstein and P Massignan, New J. Phys. **20** 013023 (2018)
[12] D Xie, W Gou, T Xiao, B Gadway and B Yan, NPJ Quantum Inf. **5** 55 (2019)
[13] Q Cheng *et. al.*, Phys. Rev. Lett. **122**, 173901 (2019).
[14] R Wakatsuki, M Ezawa, Y Tanaka and N Nagaosa, Phys. Rev. B **90**, 014505 (2014)
[15] W-L You, P Horsch and A M Oles, Phys. Rev. B **89**, 104425 (2014)
[16] R Jafari and H Johannesson, Phys. Rev. Lett. **118** 015701 (2017)
[17] C Li and A E Miroshnichenko, Physics, **1**, 2-16 (2019)
[18] B Pérez-González, M Bello, A ómez-Lón and G Platero, arXiv:1802.03973 (2018)
[19] A. Ghosh, A. M. Martin and S. Majumder, arXiv:2303.00269 (2023)
[20] B.Hetényi, Y. Pulcu and S Dogan, Phys. Rev. B **103**, 075117 (2021)
[21] Y. R. Kartik, R. R. Kumar, S. Rahul, N. Roy and S. Sarkar, Phys. Rev. B **104**, 075113 (2021)
[22] Thouless D. J., Kohomoto M., Nightingale P. and den Nijs M., Phys. Rev. Lett. **49**, 405 (1982).

[23] M. Z. Hasan and C. L. Kane, Rev. Mod. Phys. **82**, 3045 (2010).
[24] Haldane F. D. M., Phys. Rev. Lett. **61**, 2015 (1988).
[25] Jotzu G, Messer M, Desbuquois R, Lebrat M, Uehlinger T, Greif D and Esslinger T, Nature **515**, 237 (2014)
[26] M. Deb and A. K. Ghosh, J. Phys.: Condens. Matter **31** 345601 (2019)
[27] M. Deb and A. K. Ghosh, J. Phys.: Condens. Matter **32** 365601 (2020)
[28] M. Deb and A. K. Ghosh, J. Magn. Magn. Mater. **533** 167968 (2021)
[29] A. Sil and A. K. Ghosh, J. Phys.: Condens. Matter **31** 245601 (2019)
[30] A. Agarwal and J. N. Bandyopadhyay, J. Phys.: Condens. Matter **34** 305401 (2022)
[31] Y.-F. Zhao, R. Zhang, R. Mei, L.-J. Zhou, H. Yi, Y.-Q. Zhang, J. Yu, R. Xiao, K. Wang, N. Samarth, M. H. W. Chan, C.-X. Liu, and C.-Z. Chang, Nature 588, 419 (2020).
[32] L. Li, Z. Xu, and S. Chen, Phys. Rev. B 89, 085111 (2014).
[33] M Ezawa, Phys. Rev. B **104**, 235420 (2021).
[34] Hatsugai Y., Phys. Rev. Lett. **71**, 3697 (1993).
[35] Hatsugai Y., Phys. Rev. B **48**, 11851 (1993).
[36] Mook A., Henk J. and Mertig I., Phys. Rev. B **90**, 024412 (2014).
[37] T. Fukui, Y. Hatsugai and H. Suzuki, J. Phys. Soc. Japan **74**, 1674 (2005).